

Improved multispecies Dougherty collisions

Manaure Francisquez^{1,3†}, James Juno², Ammar Hakim¹,
Greg W. Hammett¹ and Darin R. Ernst³

¹Princeton Plasma Physics Laboratory, Princeton, NJ 08543, USA.

²Department of Physics & Astronomy, University of Iowa, Iowa City, IA 52242, USA.

³MIT Plasma Science and Fusion Center, Cambridge, MA 02139, USA.

(Received xx; revised xx; accepted xx)

The Dougherty model Fokker-Planck operator is extended to describe nonlinear full- f collisions between multiple species in plasmas. Simple relations for cross-species primitive moments are developed which obey conservation laws, and reproduce familiar velocity and temperature relaxation rates. This treatment of multispecies Dougherty collisions, valid for arbitrary mass ratios, avoids unphysical temperatures and satisfies the H -theorem unlike an analogous Bhatnagar-Gross-Krook operator. Formulas for both a Cartesian velocity-space and a gyroaveraged operator are provided for use in Vlasov as well as long-wavelength gyrokinetic models. We present an algorithm for the discontinuous Galerkin discretization of this operator, and provide results from relaxation and Landau damping benchmarks.

1. Introduction

Collisions play an important role in many laboratory and astrophysical plasma processes of interest. They offer a velocity-space dissipative channel in kinetic turbulence and modify transport in fusion devices, to mention a couple. In continuum kinetic models for plasmas, where small-angle collisions prevail, the effect of collisions is incorporated by the Fokker-Planck operator (FPO) (Rosenbluth *et al.* 1957). The gyrokinetic form of this operator also exists (Li & Ernst 2011; Hirvijoki *et al.* 2017; Jorge *et al.* 2019; Pan & Ernst 2019) and has been shown to agree closely with ‘model’ operators in some parameter ranges (Pan *et al.* 2020), but it can also produce significantly different results in others, particularly for instabilities and turbulence driven by the electron temperature gradient (Pan *et al.* 2021). Nevertheless, exact FPOs often prove to be analytically and numerically challenging for certain applications. Thus, there is still great interest in using simpler ‘model’ collision operators, several of which have arisen in the last several years (Abel *et al.* 2008; Sugama *et al.* 2009; Estève *et al.* 2015; Sugama *et al.* 2019; Frei *et al.* 2021). These model operators compromise accurate physics for tractability of calculations. Yet these approaches may still have sufficient complexity to deter their use, and mostly exist in linearized form for use in δf studies (e.g. Kolesnikov *et al.* (2010)).

The FPO’s drag and diffusion terms appear in terms of per unit time increments $\langle \Delta v_i \rangle_s$ and $\langle \Delta v_i \Delta v_j \rangle_s$. A particularly convenient choice is $\langle \Delta v_i \rangle_s = -\sum_r \nu_{sr} (v_i - u_{sr,i})$ and $\langle \Delta v_i \Delta v_j \rangle_s = 2 \sum_r \nu_{sr} v_{i,sr}^2 \delta_{ij}$, ν_{sr} being a suitably chosen collision frequency ($i = \{1, \dots, d_v\}$ labels the velocity component in d_v -dimensional velocity-space). This approximation leads to the simple model Fokker-Planck operator

$$\left(\frac{df_s}{dt} \right)_c = \sum_r \nu_{sr} \nabla_v \cdot [(\mathbf{v} - \mathbf{u}_{sr}) f_s + v_{i,sr}^2 \nabla_v f_s]. \quad (1.1)$$

† Email address for correspondence: mfrancis@pppl.gov

For self-species collisions $\mathbf{u}_{sr} = \mathbf{u}_s$ and $v_{t,sr}^2 = v_{t,s}^2 = T_s/m_s$ are the flow velocity and the squared thermal speed of species s , defined in terms of the velocity moments of the distribution function ($M_{0,s}$, $M_{1i,s}$, $M_{2,s}$) as

$$\begin{aligned} u_{s,i} M_{0,s} &= M_{1i,s}, \\ u_{s,i} M_{1i,s} + d_v v_{t,s}^2 M_{0,s} &= M_{2,s}, \end{aligned} \tag{1.2}$$

with such moments given by

$$\begin{aligned} M_{0,s} &= \int_{-\infty}^{\infty} f_s d^d v, \\ M_{1i,s} &= \int_{-\infty}^{\infty} v_i f_s d^d v, \\ M_{2,s} &= \int_{-\infty}^{\infty} v^2 f_s d^d v. \end{aligned} \tag{1.3}$$

This frequently used model goes by the various appellations of Kirkwood, Lenard-Bernstein or Dougherty operator. We refer to it as the LBO for simplicity. Its nonlinearity is implicit, since the primitive moments $u_{sr,i}$ and $v_{t,sr}^2$ are themselves functions of the moments of $f_{s,r}$. We also restrict ourselves to the case of velocity independent collisionality; improvements that retain this additional complexity will be explored in the future. The result is then a tractable operator which, owing to its simplicity, conservative properties, and similarity to the full FPO, is used in numerous kinetic plasma models and, with appropriate modifications, virtually every gyrokinetic model.

These attributes also make it an attractive choice for multispecies collisions. Analytic and computational studies have used Dougherty electron-ion collisions for several decades to the present day (Ong & Yu 1970; Pan *et al.* 2018; Shi *et al.* 2019). This trend however has not established the most appropriate choice of cross velocities and thermal speed, $u_{sr,i}$ and $v_{t,sr}$. A study of the universal instability, for example, used $u_{sr,i} = [m_r n_r / (m_s n_s)] u_{r,i}$ and $v_{t,sr} = v_{t,s}$, where n_s is the number density of species s (Ong & Yu 1970), while a separate analysis of ion-acoustic and drift waves later employed $u_{sr,i} = [\nu_r m_r / (\nu_{sr} m_s)] u_{s,i}$ (Ong & Yu 1973). Dougherty & Watson (1967) had proposed a linearized multispecies version of the eponymous operator with $u_{sr,i} = u_{r,i}$ and $v_{t,sr}^2 = [m_r / (m_s + m_r)] (v_{t,s}^2 + v_{t,r}^2)$. More recently Jorge *et al.* (2018) chose $u_{sr,i} = u_{s,i}$ and $v_{t,sr} = v_{t,s}$ for exploring drift-waves at arbitrary collisionality. Adding to the variance of choices, $\mathbf{u}_{ei} = \mathbf{u}_i$ and $v_{t,ei}^2 = v_{t,e}^2 + (\mathbf{u}_i - \mathbf{u}_e)^2 / 3$ were assumed in GENE and Gkeyll full- f gyrokinetic simulations of LAPD and NSTX (Pan *et al.* 2018; Shi *et al.* 2019). Furthermore, the choice of u_{sr} and $v_{t,sr}$ is related to the adoption of a particular collision frequency ν_{sr} , which Dougherty (1964) and other works left unspecified, though Dougherty & Watson (1967) show one possible choice for the linearized operator.

There has thus been a prolonged, non-systematic spread in the choice of cross-species primitive moments, $u_{sr,i}$ and $v_{t,sr}$, for multispecies collisions with the Dougherty operator. While some of the choices listed above are intuitive and appropriate in some limits, the goal of this manuscript is to more rigorously determine such cross-species primitive moments. Greene (1973) for example imposed momentum and energy conservation in electron-ion collisions with a Bhatnagar-Gross-Krook (BGK) operator (Bhatnagar *et al.* 1954), and required that the cross-species velocity and temperature relaxation rates match those given by the Boltzmann collision integral for Maxwellian distributions: the Morse relaxation rates (Morse 1963). This procedure yields relations for the $u_{sr,i}$ and $v_{t,sr}$ needed by the multispecies BGK model. Unfortunately, for unequal masses the

resulting formulae can prescribe a negative $v_{t,sr}^2$ as the relative drift $|u_{s,i} - u_{r,i}|$ increases. It has also been pointed out that, though conservative, this multispecies BGK operator cannot be proven to have (or not have) an H -theorem (Haack *et al.* 2017).

In what follows we present three different approaches to determining the Dougherty cross-species primitive moments u_{sr} and $v_{t,sr}$, drawing from the ideas of Greene (1973) and Haack *et al.* (2017) employed for the BGK operator. We begin with the presentation of these approaches in the context of Vlasov-Maxwell models (section 2). The proposed multi-species full- f nonlinear Dougherty operator is also shown to not decrease the entropy. Entropy production stands as a challenging constraint in some other collision models. For example, a modern linear δf formulation of multi-species collisions only has an H -theorem when temperatures are equal (Sugama *et al.* 2019). Furthermore, there is little work on full- f collision models; one such operator presented by Estève *et al.* (2015) has been linearized and is also only able to satisfy the H -theorem for equal temperatures. Section 2 ends with a provision of equivalent formulas for the gyroaveraged Dougherty operator which is frequently used in long-wavelength gyrokinetic simulations (Francisquez *et al.* 2020). These formulas are then implemented in the discontinuous Galerkin code Gkeyll (2020) using an algorithm described in section 3. Then, section 4 provides a series of Vlasov and gyrokinetic benchmarks illustrating the conservative properties of the algorithm and the differences between the three different strategies for selecting multispecies primitive moments. We also provide a benchmark comparing the Landau damping rate of electron Lagnmuir waves with the multispecies Dougherty operator against the results using a Fokker-Planck operator. Concluding remarks are provided in section 5.

2. Multispecies Dougherty operators

In this section we provide three different sets of formulas for the cross-species primitive moments in the LBO. The first is analogous to Greene's treatment of the BGK operator (Greene 1973) and we therefore name it the LBO-G. It introduces a free parameter that is insufficiently constrained at present. We thus complement that approach with the ideas of Haack *et al.* (2017), where two different BGK operators were proposed which independently attempt to match the FPO's momentum and thermal relaxation rates. These are the LBO-EM and LBO-ET, respectively (these operators were also recently implemented in the GENE-X code (Ulbl *et al.* 2021)). We conclude this section with similar formulas for a gyroaveraged multispecies Dougherty operator.

2.1. LBO-G

In the same vein as was done for the BGK in Greene (1973), one may enforce exact momentum and energy conservation, and use Boltzmann relaxation rates (Morse 1963) to obtain the cross-species primitive moments appropriate for Dougherty electron-ion collisions. Conservation of momentum and energy in cross-species collisions

$$\int_{-\infty}^{\infty} v_i \sum_s m_s C[f_s] d^d v = 0, \quad (2.1)$$

$$\int_{-\infty}^{\infty} \frac{1}{2} v^2 \sum_s m_s C[f_s] d^d v = 0 \quad (2.2)$$

($C[f_s]$ the right side of equation 1.1 with $r \neq s$) is obeyed pairwise and yields the relations

$$\begin{aligned} \sum_s m_s n_s \nu_{sr} \Delta u_{sr,i} &= 0, \\ \sum_s m_s n_s \nu_{sr} (d_v \Delta v_{t,sr}^2 + \mathbf{u}_s \cdot \Delta \mathbf{u}_{sr}) &= 0, \end{aligned} \quad (2.3)$$

with the sum running only over two species (r labels the species other than s), $\Delta \mathbf{u}_{sr} = \mathbf{u}_s - \mathbf{u}_{sr}$ and $\Delta v_{t,sr}^2 = v_{t,s}^2 - v_{t,sr}^2$. This system of $2(d_v + 1)$ unknowns can be closed in a number of ways; a particularly simple way is by employing the momentum and thermal relaxation rates of the full Coulomb collision operator (see equations 15 and 16 in Morse (1963)). For small-angle collisions these rates are

$$\begin{aligned} \left. \frac{\partial}{\partial t} m_s n_s u_{s,i} \right|_{\text{FPO}} &= \frac{\alpha_E}{2} (m_s + m_r) (u_{r,i} - u_{s,i}), \\ \left. \frac{\partial}{\partial t} \frac{d_v}{2} m_s n_s v_{t,s}^2 \right|_{\text{FPO}} &= \frac{\alpha_E}{2} \left[d_v (m_r v_{t,r}^2 - m_s v_{t,s}^2) + m_r (\mathbf{u}_r - \mathbf{u}_s)^2 \right]. \end{aligned} \quad (2.4)$$

The parameter α_E is inversely proportional to the energy and momentum relaxation times:

$$\alpha_E = \frac{2n_s n_r (q_s q_r)^2 \log \Lambda_{sr}}{3(2\pi)^{3/2} \epsilon_0^2 m_s m_r (v_{t,s}^2 + v_{t,r}^2)^{3/2}} \quad (2.5)$$

The right hand side of equation 2.4 originates from the Boltzmann collision integral for Coulomb interactions, truncated at the Debye length, under the premise that f_s are close to Maxwellian. The validity of the relations given below in systems where the plasma may significantly differ from Maxwellian is thus limited.

One can compute the LBO momentum and thermal relaxation rates similar to those for the FPO in equation 2.4 simply by taking velocity moments of equation 1.1. These rates are†

$$\begin{aligned} \left. \frac{\partial}{\partial t} m_s n_s u_{s,i} \right|_{\text{LBO}} &= m_s n_s \nu_{sr} (u_{sr,i} - u_{s,i}), \\ \left. \frac{\partial}{\partial t} \frac{d_v}{2} m_s n_s v_{t,s}^2 \right|_{\text{LBO}} &= d_v m_s n_s \nu_{sr} (v_{t,sr}^2 - v_{t,s}^2). \end{aligned} \quad (2.6)$$

Equating equations 2.4 and 2.6 does not fully determine u_{sr} and $v_{t,sr}^2$ because of the as-of-yet arbitrary ν_{sr} . The next step in the Greene methodology is thus to adopt a relationship between the collision frequency in the model operator and α_E , which for the BGK operator Greene took to be $\nu_{sr} = \alpha_E (m_s + m_r) / [(1 + \beta)n_s m_s]$ with the arbitrary parameter $\beta > -1$. For the LBO-G we will instead use

$$\nu_{sr} = \frac{\alpha_E (m_s + m_r)}{\delta_s (1 + \beta) m_s n_s}, \quad (2.7)$$

with $\delta_s = 2m_r n_r \nu_{rs} / (m_s n_s \nu_{sr} + m_r n_r \nu_{rs})$; it turns out that δ_s and β only appear as $\delta_s(1 + \beta)$ so their independent values do not need to be determined separately. We picked this relationship between α_E and ν_{sr} for three reasons. First, we anticipate potential difficulties guaranteeing positivity of $v_{t,sr}^2$, although we will see shortly that such problems do not arise with the Dougherty operator for many systems of interest. Second, the formulation presented here avoids the assumption $m_s n_s \nu_{sr} = m_r n_r \nu_{rs}$ used in earlier work (Greene 1973). Lastly, this definition of ν_{sr} produces relations that more easily enforce exact conservation in their discrete form.

† Dougherty & Watson (1967) have an erroneous extra factor of 3 in the equivalent momentum rate of change, their equation 2.6.

Equipped with equation 2.7 we can equate equations 2.4 and 2.6, and together with equation 2.3 a linear system in $u_{sr,i}$, $v_{t,sr}^2$, $u_{rs,i}$ and $v_{t,rs}^2$ ensues. The solution of this linear problem is

$$u_{sr,i} = u_{s,i} + \delta_s \frac{1 + \beta}{2} (u_{r,i} - u_{s,i}), \quad (2.8)$$

$$v_{t,sr}^2 = v_{t,s}^2 + \frac{\delta_s}{2} \frac{1 + \beta}{1 + \frac{m_s}{m_r}} \left[v_{t,r}^2 - \frac{m_s}{m_r} v_{t,s}^2 + \frac{(\mathbf{u}_s - \mathbf{u}_r)^2}{d_v} \right], \quad (2.9)$$

One attractive property of these cross-species primitive moments is that, contrary to their BGK counterparts, they do not suffer from the pathology of negative $v_{t,ie}^2$ at supersonic values of the relative drift $|\mathbf{u}_s - \mathbf{u}_r|$. Positivity of equation 2.9 does require however that

$$\frac{\delta_s}{2} \frac{1 + \beta}{1 + \frac{m_r}{m_s}} \left[1 - \frac{T_r}{T_s} - \frac{(\mathbf{u}_s - \mathbf{u}_r)^2}{d_v c_{s,sr}^2} \right] < 1, \quad (2.10)$$

where $c_{s,sr} = \sqrt{T_s/m_r}$. This is true for any choice of δ_s and β provided $\delta_s(1 + \beta) < 2$, even as the relative drift increases.

Despite such improvements on previous similar multispecies operators, the unspecified β parameter poses a clear disadvantage. Dougherty & Watson (1967) had already pointed out that an additional condition is needed to determine all unknowns, and therefore avoid the appearance of any free parameters. As discussed by Haack *et al.* (2017), this free parameter can modify the transport coefficients in the associated fluid models. For the BGK operator, Morse (1964) eliminated the need for β by assuming $n_s \nu_{sr} = n_r \nu_{rs}$ and requiring that the ratio of the relaxation rate for the momentum difference between the two species to that of the temperature difference be the same for both the FPO and the model operator. However the resulting multispecies BGK operator does not satisfy the H -theorem, discouraging us from pursuing that approach. A possible added constraint that may do away with such parameter is the isotropization rate due to interspecies collisions; imposing such condition is however beyond the scope of this manuscript.

2.2. LBO-EM and LBO-ET

Following the path charted by Haack *et al.* (2017) for the BGK, one could require that $u_{sr} = u_{rs}$ and $m_s v_{t,sr}^2 = m_r v_{t,rs}^2$. Then the momentum conservation constraint in equation 2.3 results in

$$u_{sr,i} = \frac{m_s n_s \nu_{sr} u_{s,i} + m_r n_r \nu_{rs} u_{r,i}}{m_s n_s \nu_{sr} + m_r n_r \nu_{rs}}, \quad (2.11)$$

while energy conservation assuming $m_s v_{t,sr}^2 = m_r v_{t,rs}^2$ yields

$$\begin{aligned} (n_s \nu_{sr} + n_r \nu_{rs}) m_s v_{t,sr}^2 &= m_s n_s \nu_{sr} v_{t,s}^2 + m_r n_r \nu_{rs} v_{t,r}^2 \\ &+ \frac{m_s n_s \nu_{sr} m_r n_r \nu_{rs}}{m_s n_s \nu_{sr} + m_r n_r \nu_{rs}} \frac{(\mathbf{u}_s - \mathbf{u}_r)^2}{d_v}. \end{aligned} \quad (2.12)$$

The next step demands that the momentum relaxation rates are the same for both the LBO and the FPO. Setting the momentum relaxation rates equal to each other

$$\begin{aligned} \frac{\partial}{\partial t} (m_s n_s u_{s,i} - m_r n_r u_{r,i}) \Big|_{\text{FPO}} &= \frac{\partial}{\partial t} (m_s n_s u_{s,i} - m_r n_r u_{r,i}) \Big|_{\text{LBO}}, \\ \alpha_E (m_s + m_r) (u_{r,i} - u_{s,i}) &= m_s n_s \nu_{sr} (u_{sr,i} - u_{s,i}) - m_r n_r \nu_{rs} (u_{rs,i} - u_{r,i}) \end{aligned} \quad (2.13)$$

and using equation 2.11 for u_{sr} one obtains the relationship

$$\alpha_E (m_s + m_r) = \frac{2m_s n_s \nu_{sr} m_r n_r \nu_{rs}}{m_s n_s \nu_{sr} + m_r n_r \nu_{rs}}. \quad (2.14)$$

On the other hand, equivalence between thermal relaxation rates

$$\begin{aligned} \frac{\partial}{\partial t} \frac{d_v}{2} (m_s n_s v_{t,s}^2 - m_r n_r v_{t,r}^2) \Big|_{\text{FPO}} &= \frac{\partial}{\partial t} \frac{d_v}{2} (m_s n_s v_{t,s}^2 - m_r n_r v_{t,r}^2) \Big|_{\text{LBO}}, \\ \alpha_E \left[d_v (m_r v_{t,r}^2 - m_s v_{t,s}^2) + \frac{m_r - m_s}{2} (\mathbf{u}_s - \mathbf{u}_r)^2 \right] &= d_v [m_s n_s \nu_{sr} (v_{t,sr}^2 - v_{t,s}^2) \\ &\quad - m_r n_r \nu_{rs} (v_{t,rs}^2 - v_{t,r}^2)], \end{aligned} \quad (2.15)$$

with the $v_{t,sr}^2$ from equation 2.12 implies that

$$\begin{aligned} \alpha_E \left[m_r v_{t,r}^2 - m_s v_{t,s}^2 + \frac{m_r - m_s}{2d_v} (\mathbf{u}_s - \mathbf{u}_r)^2 \right] &= \frac{2n_s \nu_{sr} n_r \nu_{rs}}{n_s \nu_{sr} + n_r \nu_{rs}} (m_r v_{t,r}^2 - m_s v_{t,s}^2) \\ + \frac{n_s \nu_{sr} - n_r \nu_{rs}}{n_s \nu_{sr} + n_r \nu_{rs}} \frac{m_s n_s \nu_{sr} m_r n_r \nu_{rs}}{m_s n_s \nu_{sr} + m_r n_r \nu_{rs}} \frac{(\mathbf{u}_s - \mathbf{u}_r)^2}{d_v}. \end{aligned} \quad (2.16)$$

Although they may look strongly nonlinear, one can solve equations 2.14 and 2.16 in order to obtain an expression for ν_{sr} [†]. The result is

$$\nu_{sr} = \frac{\alpha_E (m_s + m_r)}{n_s m_s} \cdot \frac{\frac{m_s - m_r}{2m_s m_r} d_v (m_r v_{t,r}^2 - m_s v_{t,s}^2) + (\mathbf{u}_s - \mathbf{u}_r)^2}{\frac{1}{m_r} d_v (m_r v_{t,r}^2 - m_s v_{t,s}^2) + (\mathbf{u}_s - \mathbf{u}_r)^2}, \quad (2.17)$$

but we can immediately notice that this can lead to negative collision frequencies in some parameter regimes; for example, the electron-ion frequency ν_{ei} with zero relative drift. This indicates that enforcing the equality of momentum and thermal relaxation rates while using the assumptions $u_{sr,i} = u_{rs,i}$ and $m_s v_{t,sr}^2 = m_r v_{t,rs}^2$ leads to unphysical behavior. We nevertheless present two slight variations in the following subsections, as was also recently done by Ulbl *et al.* (2021), in order to provide a point of reference for the LBO-G and comparing against Haack *et al.* (2017).

2.2.1. LBO-EM

Instead of trying to match both the momentum and thermal relaxation rates, we could satisfy ourselves with only attaining the same momentum relaxation rate. We can do this by employing equation 2.14, which we obtained from setting LBO and FPO momentum relaxation rates equal to each other, and further assuming that

$$m_s n_s \nu_{sr} = m_r n_r \nu_{rs}. \quad (2.18)$$

These two equations together set the collision frequency in our model to

$$\nu_{sr}^M = \alpha_E \frac{m_s + m_r}{m_s n_s} = \frac{2(m_s + m_r)(q_s q_r)^2 n_r \log A_{sr}}{3(2\pi)^{3/2} \epsilon_0^2 m_s^2 m_r (v_{t,s}^2 + v_{t,r}^2)^{3/2}}. \quad (2.19)$$

[†] Haack *et al.* (2017) state that the equivalent equations for the BGK operator are nonlinear and without a simple formula for a solution. But one can obtain such solution by casting equation 2.14 in terms of $\tau_{rs} = 1/\nu_{rs}$, solving for τ_{rs} , and substituting that into equation 56 of Haack *et al.* (2017) (the equivalent of our equation 2.16). The result is a quadratic equation for $n_s \nu_{sr}$, which can be solved.

This choice of collision frequency reduces the cross-primitive moments to

$$\begin{aligned} u_{sr,i} &= \frac{u_{s,i} + u_{r,i}}{2}, \\ v_{t,sr}^2 &= \frac{1}{1 + \frac{m_s}{m_r}} \left[v_{t,s}^2 + v_{t,r}^2 + \frac{(\mathbf{u}_s - \mathbf{u}_r)^2}{2d_v} \right]. \end{aligned} \quad (2.20)$$

We call equation 1.1 with collision frequency and cross primitive moments in equations 2.19-2.20 the LBO-EM. Compared to the equations that led to LBO-G, equation 2.19 suggests that LBO-EM is LBO-G in the limit of $\beta = 0$ and $\delta_s = 1$. In this case the cross-species flow velocity in LBO-G (equation 2.8) does reduce to that in LBO-EM, but the LBO-G cross-species thermal velocity in this limit does not equal that in equation 2.20. Interestingly for vanishing relative drifts $\beta = 1$ leads to an agreement between $v_{t,sr}^2$ for LBO-G and LBO-EM, but leads to $u_{sr,i} = u_{r,i}$, which disagrees with LBO-EM's $u_{sr,i}$. Therefore, as with BGK, LBO-EM is not a special case of LBO-G.

2.2.2. LBO-ET

Alternatively we could choose to approximately match the thermal relaxation rate of the FPO. Focusing on the temperature difference term in equation 2.4, we see that the relaxation rate due to temperature differences alone is the same for both species. We could choose to mimic this behavior, and examining equation 2.6 the conclusion would be that we have to require

$$n_s \nu_{sr} = n_r \nu_{rs}. \quad (2.21)$$

This assumption renders equations 2.11-2.12 into

$$u_{sr,i} = \frac{m_s u_{s,i} + m_r u_{r,i}}{m_s + m_r}, \quad (2.22)$$

$$v_{t,sr}^2 = \frac{1}{2} \left[v_{t,s}^2 + \frac{m_r}{m_s} v_{t,r}^2 + \frac{m_r}{m_s + m_r} \frac{(\mathbf{u}_s - \mathbf{u}_r)^2}{d_v} \right]. \quad (2.23)$$

Although we took up relation 2.21 we have not specified the collision frequency precisely yet. We can do so by returning to the thermal relaxation rate equivalence (equation 2.15) and inserting the cross-species temperature in equation 2.23. The result is[†]

$$\begin{aligned} \alpha_E \left[d_v (m_r v_{t,r}^2 - m_s v_{t,s}^2) + \frac{m_r - m_s}{2} (\mathbf{u}_s - \mathbf{u}_r)^2 \right] = \\ d_v \left[\frac{n_s \nu_{sr}}{2} \left(m_r v_{t,r}^2 - m_s v_{t,s}^2 + \frac{m_s m_r}{m_s + m_r} \frac{(\mathbf{u}_s - \mathbf{u}_r)^2}{d_v} \right) \right. \\ \left. - \frac{n_r \nu_{rs}}{2} \left(m_s v_{t,s}^2 - m_r v_{t,r}^2 + \frac{m_s m_r}{m_s + m_r} \frac{(\mathbf{u}_s - \mathbf{u}_r)^2}{d_v} \right) \right], \quad (2.24) \\ \alpha_E \left[(m_r v_{t,r}^2 - m_s v_{t,s}^2) + \frac{m_r - m_s}{2} \frac{(\mathbf{u}_s - \mathbf{u}_r)^2}{d_v} \right] = \\ \frac{n_s \nu_{sr} + n_r \nu_{rs}}{2} (m_r v_{t,r}^2 - m_s v_{t,s}^2) + \frac{1}{2} \frac{m_s m_r}{m_s + m_r} (n_s \nu_{sr} - n_r \nu_{rs}) \frac{(\mathbf{u}_s - \mathbf{u}_r)^2}{d_v}. \end{aligned}$$

These thermal relaxation rates cannot agree exactly because under the assumption

[†] We believe there's a typo in similar equations for BGK in Haack *et al.* (2017). In equation 65 of that paper the relative drift term should be multiplied by $(m_i + 3m_j)/(2m_j)$.

$n_s \nu_{sr} = n_r \nu_{rs}$ the relative drift term vanishes for this LBO, but we could at least match the response due to the temperature difference, leading to the collision frequency for this model:

$$\nu_{sr}^T = \frac{\alpha E}{n_s} = \frac{2n_r(q_s q_r)^2 \log A_{sr}}{3(2\pi)^{3/2} \epsilon_0^2 m_s m_r (v_{t,s}^2 + v_{t,r}^2)^{3/2}} \quad (2.25)$$

The operator (equation 1.1) with this collision frequency and the cross primitive moments in equations 2.22-2.23 is referred to as the LBO-ET. As with the previous operator, setting $\beta = 0$ in the LBO-G leads to the same cross-species flow velocity $u_{sr,i}$, but then the thermal speeds $v_{t,sr}$ do not agree. More importantly, we reinstate that the LBO-ET did not exactly match the FPO thermal relaxation rate because of the difference in response to relative drifts. For plasmas where the relative drifts are small relative to temperature differences (not an uncommon situation), these rates agree exactly.

2.3. H -theorem

The full FPO does not decrease entropy, i.e. it satisfies an H -theorem, and as a model Fokker-Planck operator it is desirable that this formulation of multi-species Dougherty collisions retain such property. The original paper on the multispecies Dougherty operator demonstrated a non-decreasing entropy only to second order after linearization (Dougherty & Watson 1967), hinting at the possibility that the above full- f equivalent operator could possess an H -theorem. It is in fact possible however to show that the Dougherty models for multi-species full- f collisions presented here do have an H -theorem, even for species with unequal temperatures. A more detailed proof of this statement is given in appendix B, and we give an outline of the argument here.

The total entropy $\mathcal{S} = - \sum_s \int d^d v f_s \ln f_s$ can be shown to obey

$$\dot{\mathcal{S}} = \frac{\partial \mathcal{S}}{\partial t} = - \sum_s \int d^d v \nu_{sr} (\ln f_s + 1) \nabla_v \cdot \mathbf{J}_{sr}, \quad (2.26)$$

where the flux \mathbf{J}_{sr} is the term in square brackets in equation 1.1. Using the definition of this flux and integration by parts twice together with the fact that $f_s \rightarrow 0$ faster than powers of v_i as $v_i \rightarrow \pm\infty$ one is led to

$$\dot{\mathcal{S}} = \sum_s \nu_{sr} \left(-d_v n_s + v_{t,sr}^2 \int d^d v \nabla_v f_s \cdot \nabla_v \ln f_s \right). \quad (2.27)$$

At this point we can perform a variational minimization of this functional in order to determine if that minimum is below zero (indicating a violation of thermodynamic law). For a given set of primitive moments ($n_s, u_{s,i}, v_{t,s}, u_{sr,i}, v_{t,sr}$) and the virtual displacement $\delta f_s = f_s - f_{s0}$, the response of $\dot{\mathcal{S}}$ is

$$\delta \dot{\mathcal{S}} = \sum_s v_{t,sr}^2 \int d^d v \nabla_v f_{s0} \cdot \left[\frac{2}{\delta f_s} \nabla_v \delta f_s - \frac{1}{f_{s0}} \nabla_v f_{s0} \right] \frac{\delta f_s}{f_{s0}}. \quad (2.28)$$

At an extremum in $\dot{\mathcal{S}}$ this function must vanish, and since equation 2.27 has no upper bound this extremum must be a minimum. We are also interested in virtual displacements that do not alter the moments of each distribution, that is

$$\int d^d v \mathbf{v}^k \delta f_s = 0 \quad \text{for } k \in \{0, 1, 2\}. \quad (2.29)$$

Further imposing that the displacement δf_s vanishes at infinity, $\delta \dot{\mathcal{S}} = 0$ and equations 2.28-2.29 yield the nonlinear inhomogeneous equation for the minimizing distri-

bution f_{s0}

$$|\nabla_v \ln f_{s0}|^2 + 2\nabla_v^2 \ln f_{s0} = h_0^2 + 2d_v h_1 + 2h_0 \mathbf{h}_1 \cdot \mathbf{v} + h_1^2 v^2, \quad (2.30)$$

with h_0 , \mathbf{h}_1 and h_2 undetermined linear coefficients. The solution to this equation is $f_{s0} \propto \exp(h_{0,i}v_i + h_1 v^2/2)$. Enforcing the condition that it has the same number density n_s and primitive moments ($u_{s,i}$ and $v_{t,s}$) as the original distribution, f_s , reveals that the distribution that minimizes the rate of entropy change of this operator is a Maxwellian with n_s , $u_{s,i}$ and $v_{t,s}$. The final step is to insert this distribution back into our expression for entropy change, equation 2.26, and check that the minimum entropy rate of change does not fall below zero. Such procedure results in

$$\min \left(\frac{\partial \mathcal{S}}{\partial t} \right) = d_v \sum_s \frac{n_s \nu_{sr}}{v_{t,s}^2} (v_{t,sr}^2 - v_{t,s}^2), \quad (2.31)$$

and since the procedure obtained a single minimum it must be the global minimum.

2.3.1. LBO-G H -theorem

Use the definition of $v_{t,sr}^2$ for the LBO-G model (equation 2.9) to arrive at

$$\begin{aligned} \min \left(\frac{\partial \mathcal{S}}{\partial t} \right) = \frac{\delta_s m_s n_s \nu_{sr}}{2v_{t,s}^2} \frac{1 + \beta}{m_s + m_r} \left[d_v \frac{(T_r - T_s)^2}{T_s T_r} \right. \\ \left. + \left(\frac{m_r}{m_s} \frac{1}{v_{t,s}^2} + \frac{m_s}{m_r} \frac{1}{v_{t,r}^2} \right) (\mathbf{u}_s - \mathbf{u}_r)^2 \right] \geq 0. \end{aligned} \quad (2.32)$$

We are thus led to the conclusion that the LBO-G model of full- f multispecies collisions does not decrease the entropy. This is in contrast to the BGK-G operator, for which the H -theorem could not be proven or disproven (Greene 1973; Haack *et al.* 2017).

2.3.2. LBO-EM and LBO-ET H -theorem

Using the relationship between collision frequencies for the LBO-EM (equation 2.19) and the corresponding cross-species thermal speeds one obtains

$$\min \left(\frac{\partial \mathcal{S}}{\partial t} \right) = \frac{d_v n_s \nu_{sr}}{m_s + m_r} \left[\frac{(m_r v_{t,r}^2 - m_s v_{t,s}^2)^2}{v_{t,s}^2 m_r v_{t,r}^2} + \left(\frac{m_r}{v_{t,s}^2} + \frac{m_s}{m_r} \frac{m_s + m_r}{v_{t,r}^2} \right) \frac{(\mathbf{u}_s - \mathbf{u}_r)^2}{2d_v} \right] \geq 0. \quad (2.33)$$

Similarly, using the $n_s \nu_{sr} = n_r \nu_{rs}$ assumption of the LBO-ET model and the definition of $v_{t,sr}^2$ in equation 2.23 turns equation 2.31 into

$$\min \left(\frac{\partial \mathcal{S}}{\partial t} \right) = \frac{d_v n_s \nu_{sr}}{2} \left[\frac{m_r v_{t,r}^2}{m_s v_{t,s}^2} + \frac{m_s v_{t,s}^2}{m_r v_{t,r}^2} + \left(\frac{m_r}{v_{t,s}^2} + \frac{m_s}{v_{t,r}^2} \right) \frac{1}{m_s + m_r} \frac{(\mathbf{u}_s - \mathbf{u}_r)^2}{d_v} \right] \geq 0. \quad (2.34)$$

Therefore both LBO-EM and LBO-ET models satisfy the H -theorem.

2.4. Gyroaveraged multispecies Dougherty operator

This model operator is also used by modern, long-wavelength full- f gyrokinetic codes (Pan *et al.* 2018; Gkeyll 2020) in its gyroaveraged form. Its form, conservative properties and discontinuous Galerkin discretization for self-species collisions have been presented by Francisquez *et al.* (2020). The operator can however be extended to incorporate cross-species collisions. For that purpose we write the gyroaveraged operator

acting on the guiding center distribution function $f_s(\mathbf{R}, v_{\parallel}, \mu)$ as

$$\left(\frac{\partial \mathcal{J} f_s}{\partial t}\right)_c = \sum_r \nu_{sr} \left\{ \frac{\partial}{\partial v_{\parallel}} \left[(v_{\parallel} - u_{\parallel sr}) \mathcal{J} f_s + v_{t, sr}^2 \frac{\partial \mathcal{J} f_s}{\partial v_{\parallel}} \right] + \frac{\partial}{\partial \mu} 2\mu \left[\mathcal{J} f_s + \frac{m_s v_{t, sr}^2}{B} \frac{\partial \mathcal{J} f_s}{\partial \mu} \right] \right\}, \quad (2.35)$$

where \mathcal{J} is the Jacobian of the guiding center coordinates, \mathbf{R} is the guiding center position, v_{\parallel} is the velocity along the background magnetic field and μ is the adiabatic moment; see [Francisquez *et al.* \(2020\)](#) for more details.

In order to use this multispecies gyroaveraged operator one must then determine the multispecies parallel flow velocities $u_{\parallel sr}$ and thermal speed $v_{t, sr}$. Our proposal is to use the same LBO-G (equations 2.8, 2.9), LBO-EM (equation 2.20) and LBO-ET (equations 2.22-2.23) models with this gyroaveraged operator. The only difference is that the self-species primitive moments are defined by

$$\begin{aligned} u_{\parallel s} M_{0, s} &= M_{1, s}, \\ u_{\parallel s} M_{1, s} + d_v v_{t, s}^2 M_{0, s} &= M_{2, s}, \end{aligned} \quad (2.36)$$

where $d_v = 1$ or $d_v = 3$ depending on whether one is considering v_{\parallel} - or (v_{\parallel}, μ) -space, respectively. The velocity moments in the gyroaveraged model are

$$\begin{aligned} M_{0, s} &= (2\pi/m_s) \int \mathcal{J} f_s(\mathbf{R}, v_{\parallel}, \mu) dv_{\parallel} d\mu, \\ M_{1, s} &= (2\pi/m_s) \int v_{\parallel} \mathcal{J} f_s(\mathbf{R}, v_{\parallel}, \mu) dv_{\parallel} d\mu, \\ M_{2, s} &= (2\pi/m_s) \int \left(v_{\parallel}^2 + 2\mu B/m_s \right) \mathcal{J} f_s(\mathbf{R}, v_{\parallel}, \mu) dv_{\parallel} d\mu. \end{aligned} \quad (2.37)$$

3. Discontinuous Galerkin discretization

In this section we present a DG scheme for the multispecies LBO. DG algorithms offer higher order convergence, data locality and flexibility in defining numerical fluxes to preserve physical properties of the system ([Cockburn & Shu 1998](#); [Hesthaven & Warburton 2007](#)). A DG discretization will also interface with existing Vlasov-Maxwell ([Juno *et al.* 2018](#); [Hakim & Juno 2020](#)) and gyrokinetic ([Shi *et al.* 2019](#); [Mandell *et al.* 2020](#)) DG solvers.

We present the algorithm below for a two-dimensional space consisting of one position dimension (x) and one velocity dimension (v); the extension to higher velocity dimensions is straightforward. First introduce a mesh \mathcal{T} that extends over the finite computational domain $\Omega \equiv [-L_x/2, L_x/2] \times [-L_v/2, L_v/2]$ and consists of quadrilateral cells $K_{j, k} \equiv [x_{j-1/2}, x_{j+1/2}] \times [v_{k-1/2}, v_{k+1/2}]$, with $j = 1, \dots, N_x$ and $k = 1, \dots, N_v$ labeling the cell along x and v , respectively. In each cell define a polynomial space $\mathcal{V}_{j, k}^p$ consisting of N_b orthonormalized monomials $\psi_{\ell}(x, v)$, which we take as basis functions in which dynamical fields are expanded. The discretization of equation 1.1 proceeds from a weak

or Galerkin projection; multiply equation 1.1 by ψ_ℓ and integrate over x - v in cell $K_{j,k}$:

$$\int_{K_{j,k}} \psi_\ell \left(\frac{df_s}{dt} \right)_c dx dv = \int_{x_{j-1/2}}^{x_{j+1/2}} \nu_{sr} \left(\psi_\ell G_s - \frac{\partial \psi_\ell}{\partial v} v_{t,sr}^2 \hat{f}_s \right) \Big|_{v_{k-1/2}}^{v_{k+1/2}} dx - \int_{K_{j,k}} \nu_{sr} \left[\frac{\partial \psi_\ell}{\partial v} (v - u_{sr}) f_s - \frac{\partial^2 \psi_\ell}{\partial v^2} v_{t,sr}^2 f_s \right] dx dv. \quad (3.1)$$

We used integration by parts and limited ourselves to the case of two species cross-collisions only to remove the sum in equation 1.1. The numerical flux $G_s = (v - u_{sr}) f_s + v_{t,sr}^2 \partial \hat{f}_s / \partial v$ consists of a drag term that is computed using upwinding based on the value of the $(v - u_{sr})$ at Gauss-Legendre nodes, and \hat{f}_s is a continuous distribution recovered across two cells (van Leer & Nomura 2005; van Leer & Lo 2007). This approach resulted in a conservative DG scheme in the case of self-species collisions; more details can be found in Hakim *et al.* (2020) and Francisquez *et al.* (2020). In the case of multispecies collisions it can also lead to a conservative scheme, provided the cross-species primitive moments are computed in a manner that incorporates the finite extent of velocity-space.

In what follows we will also need the velocity moments of each species (equation 1.3) in their discrete form. Discrete moments are defined as expansions in a set of N_b^x position-space polynomial basis functions $\varphi_\ell(x)$ belonging to the polynomial space \mathcal{V}_k^p in the j -th cell. The discrete velocity moments are then projections of equation 1.3 onto the φ_ℓ basis, which for $d_v = 1$ we represent as

$$M_{q,s} \doteq \int_{v_{\min}}^{v_{\max}} v^q f_s dv, \quad q \in \{0, 1, 2\}, \quad (3.2)$$

where $v_{\min} = v_{k_{\min}-1/2} = v_{1/2}$, $v_{\max} = v_{k_{\max}+1/2} = v_{N_v+1/2}$, and \doteq indicates weak equality (Hakim *et al.* 2020; Francisquez *et al.* 2020). Two fields g and h are weakly equal in the interval $I = [x_{j-1/2}, x_{j+1/2}]$ if their projections onto the basis functions in this interval are equal: $g \doteq h \Rightarrow \int_I (g - h) \varphi_\ell dx = 0$.

3.1. Discrete momentum conservation

In order to formulate a momentum conserving discretization based on equation 3.1, we can set $\psi_\ell = m_s v$ and sum over all cells along velocity-space. According to equation 2.1 this sum has to be equal and opposite to that of the other species it is colliding with. Therefore discrete momentum conservation requires that

$$\sum_k \int_{x_{j-1/2}}^{x_{j+1/2}} \left(m_s \nu_{sr} \left\{ \left(v G_s - v_{t,sr}^2 \hat{f}_s \right) \Big|_{v_{k-1/2}}^{v_{k+1/2}} - \int_{v_{k-1/2}}^{v_{k+1/2}} (v - u_{sr}) f_s dv \right\} + m_r \nu_{rs} \left\{ \left(v G_r - v_{t,rs}^2 \hat{f}_r \right) \Big|_{v_{k-1/2}}^{v_{k+1/2}} - \int_{v_{k-1/2}}^{v_{k+1/2}} (v - u_{rs}) f_r dv \right\} \right) dx = 0. \quad (3.3)$$

Carry out the velocity-space integrals and sum over all velocity-space cells. Use the fact that the numerical fluxes G_s are continuous and have opposite signs on either side of a cell boundary, and that \hat{f}_s is continuous across cell boundaries as well. Furthermore, we impose the zero-flux boundary conditions $G_s(v = v_{\max}) = G_s(v = v_{\min}) = 0$ in order to

arrive at

$$\int_{x_{j-1/2}}^{x_{j+1/2}} \left[m_s \nu_{sr} \left(v_{t,sr}^2 f_s \Big|_{v_{\min}}^{v_{\max}} + M_{1,s} - u_{sr} M_{0,s} \right) + m_r \nu_{rs} \left(v_{t,rs}^2 f_r \Big|_{v_{\min}}^{v_{\max}} + M_{1,r} - u_{rs} M_{0,r} \right) \right] dx = 0, \quad (3.4)$$

having substituted the discrete form of the velocity moments (equation 3.2). This relation is satisfied if

$$m_s \nu_{sr} \left(v_{t,sr}^2 f_s \Big|_{v_{\min}}^{v_{\max}} + M_{1,s} - u_{sr} M_{0,s} \right) + m_r \nu_{rs} \left(v_{t,rs}^2 f_r \Big|_{v_{\min}}^{v_{\max}} + M_{1,r} - u_{rs} M_{0,r} \right) \doteq 0. \quad (3.5)$$

Note that we have used the same v_{\max} and v_{\min} for both species for pedagogical reasons only. In fact since equation 3.5 is a constraint on position-space fields only, the discrete velocity-space of each species can be completely different. For completeness we state that in the d_v -dimensional case the condition for the scheme in equation 3.1 to conserve momentum is that the cross-species primitive moments u_{sr} and $v_{t,sr}$ must satisfy

$$m_s \nu_{sr} \left(M_{1i,s} - u_{sr,i} M_{0,s} + v_{t,sr}^2 \int f_s \Big|_{v_{i,\min}}^{v_{i,\max}} dS_i \right) + m_r \nu_{rs} \left(M_{1i,r} - u_{rs,i} M_{0,r} + v_{t,rs}^2 \int f_r \Big|_{v_{i,\min}}^{v_{i,\max}} dS_i \right) \doteq 0, \quad (3.6)$$

using $\int dS_i$ as an integral over the velocity-space boundaries orthogonal to the i -th velocity dimension, and the repeated index i implies summation.

3.2. Discrete energy conservation

Energy conservation will impose a secondary constraint on how the discrete cross-species primitive moments must be computed. In order to obtain such condition we substitute $\psi_\ell = m_s v^2/2$ in equation 3.1, and sum over velocity-space cells and species. This action leads to

$$\sum_k \int_{x_{j-1/2}}^{x_{j+1/2}} \left(m_s \nu_{sr} \left\{ \left(\frac{v^2}{2} G_s - v v_{t,sr}^2 \hat{f}_s \right) \Big|_{v_{k-1/2}}^{v_{k+1/2}} - \int_{v_{k-1/2}}^{v_{k+1/2}} [v(v - u_{sr}) f_s - v_{t,sr}^2 f_s] dv \right\} + m_r \nu_{rs} \left\{ \left(\frac{v^2}{2} G_r - v v_{t,rs}^2 \hat{f}_r \right) \Big|_{v_{k-1/2}}^{v_{k+1/2}} - \int_{v_{k-1/2}}^{v_{k+1/2}} [v(v - u_{rs}) f_r - v_{t,rs}^2 f_r] dv \right\} \right) dx = 0. \quad (3.7)$$

Once again we employ continuity of G_s and \hat{f}_s and boundary conditions so that after performing the velocity-space integrals and carrying out the sum over velocity-space cells this relation is transformed into

$$\int_{x_{j-1/2}}^{x_{j+1/2}} \left(m_s \nu_{sr} \left\{ v v_{t,sr}^2 f_s \Big|_{v_{\min}}^{v_{\max}} + (M_{2,s} - u_{sr} M_{1,s}) - v_{t,sr}^2 M_{0,s} \right\} + m_r \nu_{rs} \left\{ v v_{t,rs}^2 f_r \Big|_{v_{\min}}^{v_{\max}} + (M_{2,r} - u_{rs} M_{1,r}) - v_{t,rs}^2 M_{0,r} \right\} \right) dx = 0. \quad (3.8)$$

Therefore we can guarantee that our DG discretization exactly conserves energy if we enforce

$$\begin{aligned} m_s \nu_{sr} \left\{ v v_{t,sr}^2 f_s \Big|_{v_{\min}}^{v_{\max}} + (M_{2,s} - u_{sr} M_{1,s}) - v_{t,sr}^2 M_{0,s} \right\} \\ + m_r \nu_{rs} \left\{ v v_{t,rs}^2 f_r \Big|_{v_{\min}}^{v_{\max}} + (M_{2,r} - u_{rs} M_{1,r}) - v_{t,rs}^2 M_{0,r} \right\} \doteq 0 \end{aligned} \quad (3.9)$$

when computing u_{sr} , u_{rs} , $v_{t,sr}$ and $v_{t,rs}$. In the case of d_v velocity dimensions this constraint becomes

$$\begin{aligned} m_s \nu_{sr} \left[M_{2,s} - u_{sr,i} M_{1i,s} - v_{t,sr}^2 \left(d_v M_{0,s} - \int v_i f_s \Big|_{v_{i,\min}}^{v_{i,\max}} dS_i \right) \right] \\ + m_r \nu_{rs} \left[M_{2,r} - u_{rs,i} M_{1i,r} - v_{t,rs}^2 \left(d_v M_{0,r} - \int v_i f_r \Big|_{v_{i,\min}}^{v_{i,\max}} dS_i \right) \right] \doteq 0. \end{aligned} \quad (3.10)$$

We make a final comment that the substitution $\psi_\ell = m_s v^2/2$ is only valid if v^2 belongs to the space spanned by the basis, which for piecewise linear basis functions ($p = 1$) it does not. In order for the algorithm to be conservative with $p = 1$ additional precautions must be taken, a topic that is deferred to appendix C.

3.3. Discrete relaxation rates

Together with the relations $u_{sr,i} = u_{rs,i}$ and $m_s v_{t,sr}^2 = m_r v_{t,rs}^2$, and the definitions of the collision frequency given in sections 2.2.1-2.2.2, equations 3.6 and 3.10 are all one needs to compute the cross-primitive moments for the LBO-EM and LBO-ET. The LBO-G however needs to further incorporate the equivalence between the momentum and thermal relaxation rates of the FPO (equation 2.4) and those of the LBO (equations 2.6) in the discrete sense. First we obtain the weak form of equation 2.13 by projecting it onto the ψ_ℓ basis function:

$$\begin{aligned} m_s \nu_{sr} \left(M_{1i,s} - u_{sr,i} M_{0,s} + v_{t,sr}^2 \int f_s \Big|_{v_{i,\min}}^{v_{i,\max}} dS_i \right) \\ - m_r \nu_{rs} \left(M_{1i,r} - u_{rs,i} M_{0,r} + v_{t,rs}^2 \int f_r \Big|_{v_{i,\min}}^{v_{i,\max}} dS_i \right) \doteq \alpha_E (m_s + m_r) (u_{s,i} - u_{r,i}), \end{aligned} \quad (3.11)$$

where we used the same series of steps that led to equation 3.6.

The equivalent condition on the thermal relaxation rates necessitates the discrete thermal speed moment of the LBO. We can obtain it by substituting $\psi_\ell = m_s (v - u_s)^2/2$ into the weak scheme in equation 3.1 and summing over velocity-space cells, resulting in

$$\begin{aligned} \sum_k \int_{K_{j,k}} \frac{m_s}{2} (v - u_s)^2 \left(\frac{df_s}{dt} \right)_c dx dv = \sum_k \int_{x_{j-1/2}}^{x_{j+1/2}} m_s \nu_{sr} \left\{ \left[\frac{1}{2} (v - u_s)^2 G_s \right. \right. \\ \left. \left. - (v - u_s) v_{t,sr}^2 \hat{f}_s \right] \Big|_{v_{k-1/2}}^{v_{k+1/2}} - \int_{v_{k-1/2}}^{v_{k+1/2}} [(v - u_s)(v - u_{sr}) - v_{t,sr}^2] f_s dv \right\} dx. \end{aligned} \quad (3.12)$$

Performing the velocity-space integrals, carrying out the k -sum, accounting for the continuity of G_s and \hat{f}_s and using the zero-flux boundary conditions on G_s ushers us to

$$\begin{aligned} \sum_k \int_{K_{j,k}} \left(\frac{d(m_s n_s v_{t,s}^2/2)}{dt} \right)_c dx dv = \int_{x_{j-1/2}}^{x_{j+1/2}} m_s \nu_{sr} \left\{ \left[- (v - u_s) v_{t,sr}^2 f_s \right] \Big|_{v_{\min}}^{v_{\max}} \right. \\ \left. - [M_{2,s} - u_s M_{1,s} + u_{sr} (u_s M_{0,s} - M_{1,s}) - v_{t,sr}^2 M_{0,s}] \right\} dx, \end{aligned} \quad (3.13)$$

or in the d_v -dimensional velocity space

$$\sum_k \int_{K_{j,k}} \left(\frac{d(m_s n_s v_{t,s}^2/2)}{dt} \right)_c dx dv = \int_{x_{j-1/2}}^{x_{j+1/2}} m_s \nu_{sr} \left\{ v_{t,sr}^2 \int_{v_{i,\min}}^{v_{i,\max}} [-(v_i - u_{s,i}) f_s] dS_i \right. \\ \left. - [M_{2,s} - u_{s,i} M_{1i,s} + u_{sr,i} (u_{s,i} M_{0,s} - M_{1i,s}) - v_{t,sr}^2 d_v M_{0,s}] \right\} dx, \quad (3.14)$$

where once again the repeated index i implies summation. Equipped with this formula we can write down the discrete equivalence between thermal relaxation rates (equation 2.15) as

$$m_s \nu_{sr} \left\{ v_{t,sr}^2 \int_{v_{i,\min}}^{v_{i,\max}} [-(v_i - u_{s,i}) f_s] dS_i \right. \\ \left. - [M_{2,s} - u_{s,i} M_{1i,s} + u_{sr,i} (u_{s,i} M_{0,s} - M_{1i,s}) - v_{t,sr}^2 d_v M_{0,s}] \right\} \\ - m_r \nu_{rs} \left\{ v_{t,rs}^2 \int_{v_{i,\min}}^{v_{i,\max}} [-(v_i - u_{r,i}) f_r] dS_i \right. \\ \left. - [M_{2,r} - u_{r,i} M_{1i,r} + u_{rs,i} (u_{r,i} M_{0,r} - M_{1i,r}) - v_{t,rs}^2 d_v M_{0,r}] \right\} \\ \doteq \alpha_E \left[d_v (m_r v_{t,r}^2 - m_s v_{t,s}^2) + \frac{m_r - m_s}{2} (\mathbf{u}_s - \mathbf{u}_r)^2 \right] \quad (3.15)$$

The two discrete relaxation rate equivalences in equations 3.11 and 3.15 in conjunction with the discrete momentum and energy conservation constraints (equations 3.6 and 3.10) provide the four equations for the calculation of the $u_{sr,i}$, $u_{rs,i}$, $v_{t,sr}$, $v_{t,rs}$ unknowns in the LBO-G, provided a value of β . Equations 3.11 and 3.15 however are written in terms of the self primitive moments (e.g. $u_{s,i}$, $v_{t,s}$) of each species, imbuing such equations with some ambiguity as to whether the calculation of self-primitive moments should include the corrections from velocity-space boundaries or not (Hakim *et al.* 2020; Francisquez *et al.* 2020). We therefore opt to instead write those relations in terms of the velocity moments as follows

$$m_s \nu_{sr} \left(M_{1i,s} - u_{sr,i} M_{0,s} + v_{t,sr}^2 \int_{v_{i,\min}}^{v_{i,\max}} f_s dS_i \right) \\ - m_r \nu_{rs} \left(M_{1i,r} - u_{rs,i} M_{0,r} + v_{t,rs}^2 \int_{v_{i,\min}}^{v_{i,\max}} f_r dS_i \right) \\ \doteq \frac{\alpha_E (m_s + m_r)}{M_{0,s} M_{0,r}} (M_{0,r} M_{1i,s} - M_{0,s} M_{1i,r}), \\ m_s \nu_{sr} \left\{ -v_{t,sr}^2 \int_{v_{i,\min}}^{v_{i,\max}} (v_i - u_{s,i}) f_s dS_i \right. \\ \left. - [M_{2,s} - u_{s,i} M_{1i,s} + u_{sr,i} (u_{s,i} M_{0,s} - M_{1i,s}) - v_{t,sr}^2 d_v M_{0,s}] \right\} \\ - m_r \nu_{rs} \left\{ -v_{t,rs}^2 \int_{v_{i,\min}}^{v_{i,\max}} (v_i - u_{r,i}) f_r dS_i \right. \\ \left. - [M_{2,r} - u_{r,i} M_{1i,r} + u_{rs,i} (u_{r,i} M_{0,r} - M_{1i,r}) - v_{t,rs}^2 d_v M_{0,r}] \right\} \\ \doteq \frac{\alpha_E}{M_{0,s} M_{0,r}} [m_r M_{0,s} (M_{2,r} - u_{r,i} M_{1i,r}) - m_s M_{0,r} (M_{2,s} - u_{s,i} M_{1i,s}) \\ + \frac{m_r - m_s}{2} (u_{s,i} - u_{r,i}) (M_{0,r} M_{1i,s} - M_{0,s} M_{1i,r})]. \quad (3.16)$$

The division by $M_{0,s} M_{0,r}$ on the right side of these equations is to be performed weakly (Hakim *et al.* 2020) in order to avoid aliasing errors.

3.4. Summary of discrete equations

In summary, in order for the algorithm based on equation 3.1 to conserve momentum and energy the discrete cross primitive moments are computed using the conservation constraints

$$\begin{aligned}
& m_s \nu_{sr} \left(u_{sr,i} M_{0,s} - v_{t,sr}^2 \int f_s \Big|_{v_{i,\min}}^{v_{i,\max}} dS_i \right) \\
& + m_r \nu_{rs} \left(u_{rs,i} M_{0,r} - v_{t,rs}^2 \int f_r \Big|_{v_{i,\min}}^{v_{i,\max}} dS_i \right) \doteq m_s \nu_{sr} M_{1i,s} + m_r \nu_{rs} M_{1i,r}, \\
& m_s \nu_{sr} \left[u_{sr,i} M_{1i,s} + v_{t,sr}^2 \left(d_v M_{0,s} - \int v_i f_s \Big|_{v_{i,\min}}^{v_{i,\max}} dS_i \right) \right] \\
& + m_r \nu_{rs} \left[u_{rs,i} M_{1i,r} + v_{t,rs}^2 \left(d_v M_{0,r} - \int v_i f_r \Big|_{v_{i,\min}}^{v_{i,\max}} dS_i \right) \right] \doteq m_s \nu_{sr} M_{2,s} + m_r \nu_{rs} M_{2,r}.
\end{aligned} \tag{3.17}$$

Additionally, the LBO-EM and LBO-ET use $u_{sr,i} = u_{rs,i}$ and $m_s v_{t,sr}^2 = m_r v_{t,rs}^2$, respectively, as well as their corresponding collision frequencies (equations 2.19 and 2.25). When the discrete expansions are inserted in equation 3.17 one is faced with a linear problem of size $(d_v + 1)N_b^x$ that must be solved in every position-space cell (N_b^x is the number of monomials of the basis spanning position-space). The LBO-G on the other hand uses the equality between discrete LBO relaxation rates and the FPO relaxation rates:

$$\begin{aligned}
& m_s \nu_{sr} \left(u_{sr,i} M_{0,s} - v_{t,sr}^2 \int f_s \Big|_{v_{i,\min}}^{v_{i,\max}} dS_i \right) - m_r \nu_{rs} \left(u_{rs,i} M_{0,r} - v_{t,rs}^2 \int f_r \Big|_{v_{i,\min}}^{v_{i,\max}} dS_i \right) \\
& \doteq m_s \nu_{sr} M_{1i,s} - m_r \nu_{rs} M_{1i,r} + \frac{\alpha_E (m_s + m_r)}{M_{0,s} M_{0,r}} (M_{0,s} M_{1i,r} - M_{0,r} M_{1i,s}),
\end{aligned} \tag{3.18}$$

$$\begin{aligned}
& m_s \nu_{sr} \left\{ u_{sr,i} (M_{1i,s} - u_{s,i} M_{0,s}) + v_{t,sr}^2 \left[d_v M_{0,s} - \int (v_i - u_{s,i}) f_s \Big|_{v_{i,\min}}^{v_{i,\max}} dS_i \right] \right\} \\
& - m_r \nu_{rs} \left\{ u_{rs,i} (M_{1i,r} - u_{r,i} M_{0,r}) + v_{t,rs}^2 \left[d_v M_{0,r} - \int (v_i - u_{r,i}) f_r \Big|_{v_{i,\min}}^{v_{i,\max}} dS_i \right] \right\} \\
& \doteq m_s \nu_{sr} (M_{2,s} - u_{s,i} M_{1i,s}) - m_r \nu_{rs} (M_{2,r} - u_{r,i} M_{1i,r}) \\
& + \frac{\alpha_E}{M_{0,s} M_{0,r}} [m_r M_{0,s} (M_{2,r} - u_{r,i} M_{1i,r}) - m_s M_{0,r} (M_{2,s} - u_{s,i} M_{1i,s}) \\
& + \frac{m_r - m_s}{2} (u_{s,i} - u_{r,i}) (M_{0,r} M_{1i,s} - M_{0,s} M_{1i,r})],
\end{aligned} \tag{3.19}$$

where the relationship between α_E and ν_{sr} is given by equation 2.7. Therefore for the LBO-G equations 3.17-3.19 signify a $2(d_v + 1)N_b^x$ linear problem that must be solved in every position-space cell.

3.4.1. Discrete equations for the gyroaveraged operator

In section 2.4 we introduced the gyroaveraged cross-species LBO. Its discretization follows that outlined in Francisquez *et al.* (2020) and the calculation of the cross primitive moments $u_{\parallel sr}$ and $v_{t,sr}$ is similar to that done for the non-gyroaveraged operator. The main differences arise from the fact that moments are defined via $v_{\parallel} \mu$ integrals (e.g. equation 2.37) and that the momentum density $M_{1\parallel,s}$ is a scalar instead of a vectorial quantity. The equations that arise from momentum and energy conservation in the

gyroaveraged case are thus

$$\begin{aligned} & m_s \nu_{sr} \left(M_{1\parallel,s} - u_{\parallel sr} M_{0,s} + v_{t,sr}^2 \frac{2\pi}{m_s} \int \mathcal{J} \hat{f}_s \Big|_{v_{\parallel \min}}^{v_{\parallel \max}} d\mu \right) \\ & + m_r \nu_{rs} \left(M_{1\parallel,r} - u_{\parallel rs} M_{0,r} + v_{t,rs}^2 \frac{2\pi}{m_r} \int \mathcal{J} \hat{f}_r \Big|_{v_{\parallel \min}}^{v_{\parallel \max}} d\mu \right) \doteq 0, \end{aligned} \quad (3.20)$$

$$\begin{aligned} & m_s \nu_{sr} \left[M_{2,s} - u_{\parallel sr} M_{1\parallel,s} \right. \\ & \quad \left. - v_{t,sr}^2 \left(3M_{0,s} - \frac{2\pi}{m_s} \int v_{\parallel} \mathcal{J} \hat{f}_s \Big|_{v_{\parallel \min}}^{v_{\parallel \max}} d\mu - \frac{2\pi}{m_s} \int 2\mu \mathcal{J} \hat{f}_s \Big|_{\mu_{\min}}^{\mu_{\max}} dv_{\parallel} \right) \right] \\ & + m_r \nu_{rs} \left[M_{2,r} - u_{\parallel rs} M_{1\parallel,r} \right. \\ & \quad \left. - v_{t,rs}^2 \left(3M_{0,r} - \frac{2\pi}{m_r} \int v_{\parallel} \mathcal{J} \hat{f}_r \Big|_{v_{\parallel \min}}^{v_{\parallel \max}} d\mu - \frac{2\pi}{m_r} \int 2\mu \mathcal{J} \hat{f}_r \Big|_{\mu_{\min}}^{\mu_{\max}} dv_{\parallel} \right) \right] \doteq 0, \end{aligned} \quad (3.21)$$

For the gyroaveraged LBO-EM and LBO-ET equations 3.20-3.21, and the relations $u_{\parallel sr} = u_{\parallel rs}$ and $m_s v_{t,sr}^2 = m_r v_{t,rs}^2$, is all that is needed to compute the cross primitive moments. This requires a solution to a linear problem of size $2N_b^x$ in each position-space cell. In the case of the LBO-G operator we make use of the discrete moment relaxation equations once again, as in equations 3.18-3.19 but using the gyroaveraged moments instead:

$$\begin{aligned} & m_s \nu_{sr} \left(u_{\parallel sr} M_{0,s} - v_{t,sr}^2 \frac{2\pi}{m_s} \int \mathcal{J} \hat{f}_s \Big|_{v_{\parallel \min}}^{v_{\parallel \max}} d\mu \right) - m_r \nu_{rs} \left(u_{\parallel rs} M_{0,r} - v_{t,rs}^2 \frac{2\pi}{m_r} \int \mathcal{J} \hat{f}_r \Big|_{v_{\parallel \min}}^{v_{\parallel \max}} d\mu \right) \\ & \doteq m_s \nu_{sr} M_{1\parallel,s} - m_r \nu_{rs} M_{1\parallel,r} + \frac{\alpha E (m_s + m_r)}{M_{0,s} M_{0,r}} (M_{0,s} M_{1\parallel,r} - M_{0,r} M_{1\parallel,s}), \end{aligned} \quad (3.22)$$

$$\begin{aligned} & m_s \nu_{sr} \left\{ u_{\parallel sr} (M_{1\parallel,s} - u_{\parallel s} M_{0,s}) \right. \\ & \quad \left. + v_{t,sr}^2 \left[3M_{0,s} - \frac{2\pi}{m_s} \int (v_{\parallel} - u_{\parallel s}) \mathcal{J} \hat{f}_s \Big|_{v_{\parallel \min}}^{v_{\parallel \max}} d\mu - \frac{2\pi}{m_s} \int 2\mu \mathcal{J} \hat{f}_s \Big|_{\mu_{\min}}^{\mu_{\max}} dv_{\parallel} \right] \right\} \\ & - m_r \nu_{rs} \left\{ u_{\parallel rs} (M_{1\parallel,r} - u_{\parallel r} M_{0,r}) \right. \\ & \quad \left. + v_{t,rs}^2 \left[3M_{0,r} - \frac{2\pi}{m_r} \int (v_{\parallel} - u_{\parallel r}) \mathcal{J} \hat{f}_r \Big|_{v_{\parallel \min}}^{v_{\parallel \max}} d\mu - \frac{2\pi}{m_r} \int 2\mu \mathcal{J} \hat{f}_r \Big|_{\mu_{\min}}^{\mu_{\max}} dv_{\parallel} \right] \right\} \\ & \doteq m_s \nu_{sr} (M_{2,s} - u_{\parallel s} M_{1\parallel,s}) - m_r \nu_{rs} (M_{2,r} - u_{\parallel r} M_{1\parallel,r}) \\ & \quad + \frac{\alpha E}{M_{0,s} M_{0,r}} [m_r M_{0,s} (M_{2,r} - u_{\parallel r} M_{1\parallel,r}) - m_s M_{0,r} (M_{2,s} - u_{\parallel s} M_{1\parallel,s}) \\ & \quad + \frac{m_r - m_s}{2} (u_{\parallel s} - u_{\parallel r}) (M_{0,r} M_{1\parallel,s} - M_{0,s} M_{1\parallel,r})], \end{aligned} \quad (3.23)$$

where once again weak division by $M_{0,s} M_{0,r}$ on the right side of these equations assumed (Hakim *et al.* 2020) in order to avoid aliasing errors. In equations 3.20-3.23 we assumed a $v_{\parallel}\mu$ simulation such that $d_v = 3$. For a v_{\parallel} simulation the 3 in front of $M_{0,s}$ and $M_{0,r}$ would be simply a 1, $(2\pi/m) \int d\mu$ integrals would vanish and so would the $2\mu \mathcal{J} \hat{f}$ terms. In either case the gyroaveraged LBO-G requires inverting a matrix with $4N_b^x \times 4N_b^x$ matrix in each configuration space cell.

4. Benchmarks and results

The algorithm introduced in section 3 has been implemented in the DG Vlasov-Maxwell (Juno *et al.* 2018; Hakim & Juno 2020) and gyrokinetic (Shi *et al.* 2019;

Mandell *et al.* 2020) solvers of the Gkeyll computational plasma physics framework (Gkeyll 2020). In order to demonstrate the algorithm's properties and test the implementation we have run a number of tests and we here present the results of three of them: section 4.1 contains basic tests showing the conservative properties of the algorithm, section 4.2 contains four dimensional Vlasov-Maxwell simulations of collisional Landau damping of an electron plasma wave, and section 4.3 uses the gyrokinetic solver to explore velocity and temperature relaxation. All the input files used to generate these results are available online (see appendix A).

4.1. Conservation tests

4.1.1. Vlasov LBO conservation

We check that momentum and energy are indeed conserved by our discrete scheme by initiating two populations of electrons and protons with an arbitrary non-Maxwellian distribution function given by:

$$f_s(\mathbf{v}, t = 0) = a [1 + d \cos(k_s v)] \exp \left[-\frac{(\mathbf{v} - \mathbf{b}_s)^2}{2\sigma_s^2} \right], \quad (4.1)$$

with $a = 7 \times 10^{19}$, $d = 0.5$, $k_s = \pi/v_{t,s}$, $\sigma_s = v_{t,s}$, $\mathbf{b}_e = \{v_{t,e}/2, -v_{t,e}/2, 0\}$, $\mathbf{b}_i = \{3v_{t,i}/2, 3v_{t,i}/2, v_{t,i}/2\}$ with $v_{t,s} = \sqrt{T_{s0}/m_s}$, and $T_{e0} = 40$ eV and $T_{i0} = 80$ eV. We discretize these distribution functions in phase spaces restricted to $[-1, 1] \times [-5v_{t,s}, 5v_{t,s}]^{d_v}$ and meshed with $1 \times N_v^{d_v}$ cells. We show conservation properties for both piecewise linear ($p = 1$) and piecewise quadratic ($p = 2$) Serendipity basis functions (Juno *et al.* 2018); higher order basis functions may also be used but the results do not change. For the same reason we use a single cell in position-space; the results in this section are independent of position-space dimensionality although we checked such cases anyway to make sure there are no errors in the implementation.

We time-integrate the cross-species collision terms (no self-species collisional or collisionless terms are included here) with constant collision frequency using a strong-stability preserving (SSP) third-order Runge-Kutta method (RK3). As electrons and ions collide with each other their temperatures and flow velocities relax to a common value, a process that is more carefully benchmarked in section 4.3. We also see that whatever anisotropies were present at $t = 0$ go away on the ν_{sr}^{-1} time scale. In figure 1, for example, we illustrate the isotropization of the electrons after several $(\nu_{ei}^M)^{-1}$ periods as they collide with the ions using the LBO-EM, but since ν_{ie} is smaller by m_e/m_i the ions will take much longer to isotropize as they collide with the electrons.

We ran this simulation for $d_v = \{1, 2, 3\}$, $p = \{1, 2\}$ and using both the LBO-EM and the LBO-G. The ability to conserve the first three volume-integrated velocity moments of the distribution function was quantified in each case by integrating the equations for N_t time steps, and computing the relative error per time step in the volume integrated particle, momentum and kinetic energy density. The relative error per time step in the number density M_0 is given by

$$E_{r,M_0} = \frac{1}{N_t} \frac{\langle M_{0e} + M_{0i} \rangle (t = N_t \Delta t) - \langle M_{0e} + M_{0i} \rangle (t = 0)}{\langle M_{0e} + M_{0i} \rangle (t = 0)}, \quad (4.2)$$

where $\langle \cdot \rangle$ indicates a volume average and $N_t = 10^4$. The relative error per time step in

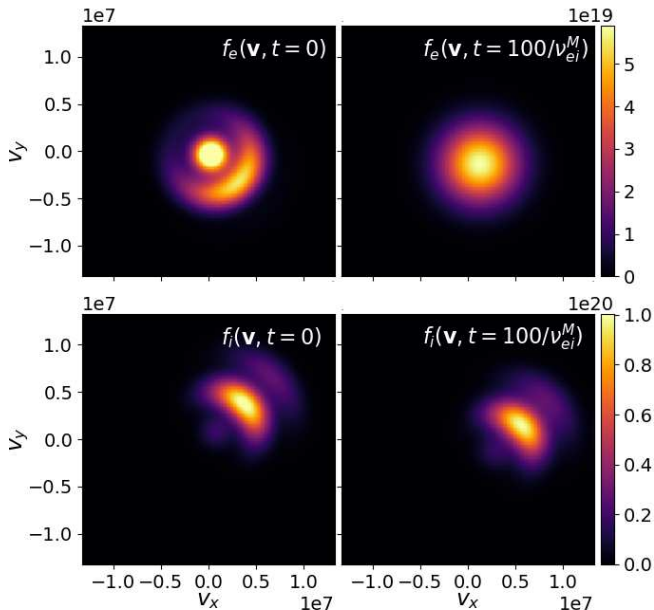


Figure 1: Initial and final (after $\nu_{ei}^M t = 100$) electron and ion distribution functions as they collide with each other with the LBO-EM model using 1×64^2 cells and a $p = 2$ Serendipity basis. Initial conditions are given in equation 4.1. Colorbars are normalized to the extrema at $\nu_{ei}^M t = 100$.

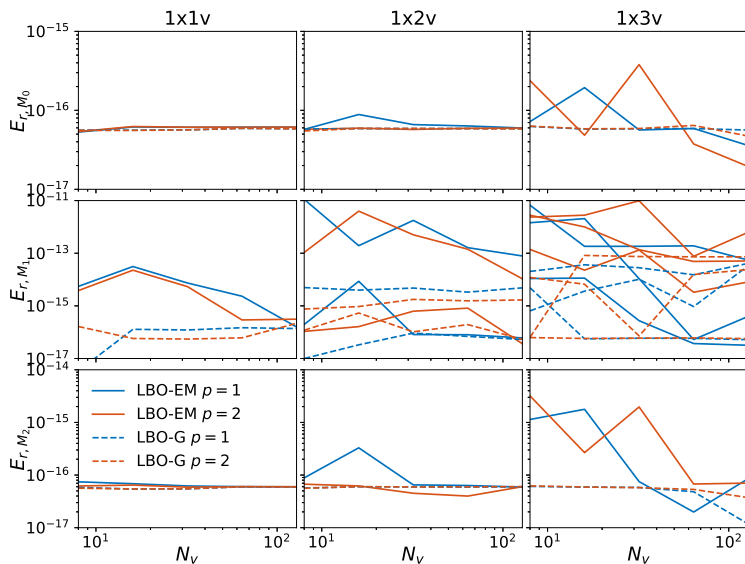


Figure 2: Relative error per time step in number density (top row), momentum density in each direction (middle row) and kinetic energy density (bottom row). The middle row plots contain d_v lines for each operator and p , corresponding to the error per time step in the conservation of momentum along each direction.

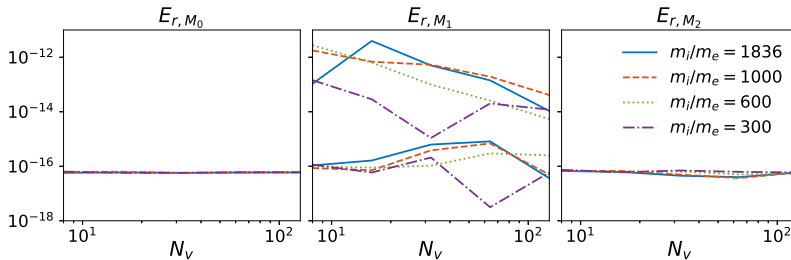


Figure 3: Relative error per time step in number density (left), momentum density in each direction (center) and kinetic energy density (right) in two-dimensional velocity space ($d_v = 2$).

momentum and kinetic energy conservation take into account the mass of each species:

$$E_{r,M_{1k}} = \frac{1}{N_t} \frac{\langle m_e M_{1e,k} + m_i M_{1i,k} \rangle (t = N_t \Delta t) - \langle m_e M_{1e,k} + m_i M_{1i,k} \rangle (t = 0)}{\langle m_e M_{1e,k} + m_i M_{1i,k} \rangle (t = 0)}, \quad (4.3)$$

$$E_{r,M_2} = \frac{1}{N_t} \frac{\langle \frac{1}{2} m_e M_{2e} + \frac{1}{2} m_i M_{2i} \rangle (t = N_t \Delta t) - \langle \frac{1}{2} m_e M_{2e} + \frac{1}{2} m_i M_{2i} \rangle (t = 0)}{\langle \frac{1}{2} m_e M_{2e} + \frac{1}{2} m_i M_{2i} \rangle (t = 0)}. \quad (4.4)$$

The results as a function of velocity space resolution (i.e. N_v) are given in figure 2. The middle row plots have d_v lines for each operator and polynomial order p because the relative error per time step in the volume-integrated momentum density is measured along each direction separately. In all cases we see that the errors in momentum conservation per time step remain of the order of machine precision. This is true even for the simulations with piece-wise linear basis functions or very coarse velocity-space meshes. The LBO-ET uses the same algorithm and implementation as LBO-EM but with a different collision frequency, so its conservation errors are similar to those of the LBO-EM shown here.

These conservation properties do not depend on the large mass disparity between ions and electrons; the algorithm's ability to conserve the velocity moments is also independent of the mass ratio. We provide as an example the $d_v = 2$ and $p = 2$ simulation with the LBO-EM, scanning the number of velocity space cells in one direction (N_v) and using the mass ratios $m_i/m_e = \{300, 600, 1000, 1836\}$. The conservation errors for these simulations are provided in figure 3, once again shown that for all mass ratios and resolutions used, the error per time step in the volume integrated velocity moments remains of the order of machine precision.

4.1.2. Gyroaveraged LBO conservation

Similar tests were run with the gyroaveraged version of the LBO operators in order to guarantee that the algorithm remains conservative in that case as well. For these tests we initialize the ion and electron distribution functions with

$$f_s(v_{\parallel}, \mu, t = 0) = \frac{a [1 + d \cos(k_s v)]}{(2\pi\sigma_s^2)^{3/2}} \exp \left[-\frac{(v_{\parallel} - b_s)^2 + 2\mu B m_s}{2\sigma_s^2} \right], \quad (4.5)$$

and the parameters $B = 1.2$ T, $a = 7 \times 10^{19}$, $d = 0.5$, $k_s = \pi/v_{t,s}$, $\sigma_s = v_{t,s}$, $b_e = 5v_{t,i}/4$, $b_i = v_{t,i}$, $v_{t,s} = \sqrt{T_{s0}/m_s}$, $T_{e0} = 40$ eV and $T_{i0} = 80$ eV. The phase space $[-1, 1] \times [-5v_{t,s}, 5v_{t,s}] \times [0, m_s (5v_{t,s})^2 / (2B)]$ is meshed with $1 \times N_v^2$ cells and functions are expanded on piecewise linear ($p = 1$) or piecewise quadratic ($p = 2$) Serendipity basis.

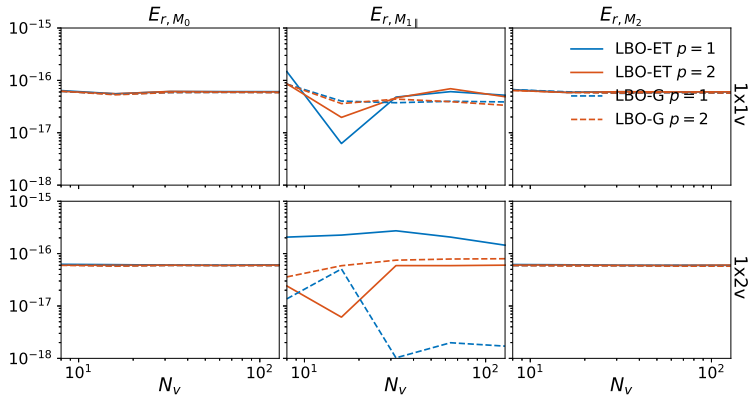


Figure 4: Relative error per time step in number density (left), momentum density (center) and kinetic energy density (right) as a function of the number of cells along one direction of velocity space (N_v) for the gyroaveraged LBO-ET (solid) and LBO-G (dashed). Top row contains tests with v_{\parallel} -space only, while the bottom row contains tests in $v_{\parallel} - \mu$ space.

We allow the electrons and ions to collide with each other but not with themselves, and we do not apply the collisionless terms either. The cross-species collision terms were integrated in time for 10^4 time steps using a third-order SSP RK3, and we computed the relative error per time step in the volume integrated velocity moments as in section 4.1.2. The results in figure 4 demonstrate how the relative error per time step in the conservation of velocity moments stays of order of machine precision for all velocity-space resolutions, and even for $p = 1$. Figure 4 gives conservation errors for the LBO-ET and the LBO-G; the LBO-EM has similar conservative properties as the LBO-ET since it only differs by the definition of the collision frequency.

4.2. Landau damping of electron Langmuir waves

A seminal test-bed for collision operators is the Landau damping of plasma waves across the collisional range. We pursued this analysis to examine the effect that these collision models have on the Landau damping rate of electrostatic electron Langmuir waves. For this purpose we employ the Vlasov-Maxwell solver in `Gkeyll` (Juno *et al.* 2018; Hakim & Juno 2020) with the self-species collision terms (Hakim *et al.* 2020) and the multi-species collision models described in this work. The hydrogen ions are fixed in time so the equations solved are

$$\frac{\partial f_e}{\partial t} + \mathbf{v} \cdot \nabla f_e - \mathbf{E} \cdot \nabla_{\mathbf{v}} f_e = \sum_{r=e,i} \nu_{er} \nabla_{\mathbf{v}} \cdot [(\mathbf{v} - \mathbf{u}_{er}) f_e + v_{ter}^2 \nabla_{\mathbf{v}} f_e], \quad (4.6)$$

$$\frac{\partial \mathbf{E}}{\partial t} = -\mathbf{J}, \quad (4.7)$$

where we used normalized units[†], the current density is given by $\mathbf{J} = -\mathbf{M}_{1e}$, and we solve equation 4.7 in a way that keeps the simulation electrostatic[‡]. We use four-dimensional simulations with the phase-space $[-\pi/k, \pi/k] \times [-5v_{t,e}, 5v_{t,e}]^3$ discretized by 16×36^3 cells and $p = 2$ basis functions, for the wavenumber $k\lambda_{De} = 0.3$, with λ_{De} being the

[†] <https://gkeyll.readthedocs.io/en/latest/dev/vlasov-normalizations.html>

[‡] <http://ammar-hakim.org/sj/je/je33/je33-buneman.html>

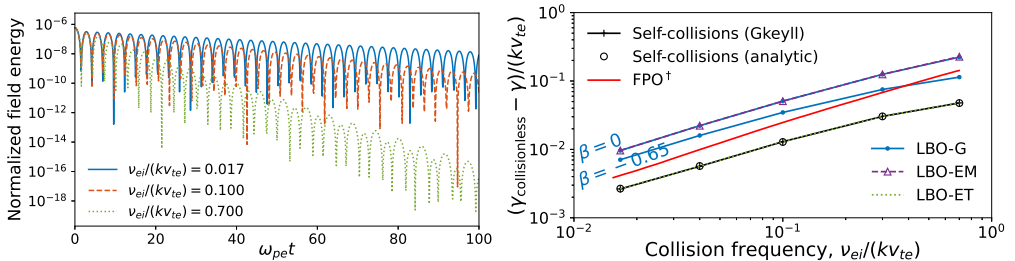


Figure 5: Left: normalized volume integrated field energy in simulations of electron Langmuir waves as they Landau damp over time. Right: damping rates of electron Langmuir waves given as the offset from the collisionless value of $\gamma_{\text{collisionless}}/\omega_{pe} = -1.247 \times 10^{-2}$ for the LBO-G with $\beta = 0$ and $\beta = -0.65$ (blue circles), the LBO-EM (purple triangles) and the LBO-ET (dotted green) compared to those with a full FPO (Jorge *et al.* 2019) (solid red). If using only self-collisions, numerical Gkeyll data (black crosses) agrees with theory (black circles).

electron Debye length. We confirmed that the resolution used is the minimum needed to obtain converged results by scanning the position- and velocity-space resolution as well as the velocity-space extents. The static ions have the normalized density $n_i(x) = 1$ while the electrons are initialized with a non-drifting Maxwellian distribution that has the temperature $T_e = 1 = T_i$ and the density $n_e(x, t = 0) = 1 + \alpha \cos(kx)$, with $\alpha = 10^{-4}$. The electric field is initialized in a manner consistent with Poisson's equation: $\mathbf{E} = -\hat{\mathbf{x}} \alpha \sin(kx)/k$.

As the simulation proceeds we see the amplitude of the electrostatic wave damp, which can be appreciated by examining the volume integrated field energy over time as shown in figure 5(left). We can quantify the rate at which these waves damp and plot it as a function of collision frequency as is done in figure 5(right). If one were to only use self-species collisions one would obtain the results shown with black crosses, and for that case the equations are sufficiently simple that one can obtain an analytic dispersion relation (Anderson & O'Neil 2007; Francisquez *et al.* 2020) which agrees well with the numerical results (black circles), providing additional confidence in the Gkeyll implementation. When we introduce electron-ion collisions obtaining analytic growth rates is more difficult. So we instead compare the results obtained with the LBO-G (solid blue), the LBO-EM (dashed purple) and the LBO-ET (dotted green) with previously reported results for the FPO (Jorge *et al.* 2019).

The LBO-G simulations were performed using $\nu_{ei}^G = \sqrt{2}\nu_{ee} (= (m_i/m_e)\nu_{ie})$ since this is the relationship assumed in the reference FPO work (Jorge *et al.* 2019). Figure 5(right) suggests that the LBO-G can provide a more accurate description of this kinetic phenomenon than, say, using self-species collisions only. There is the caveat however that we have not established from first principles what the most suitable choice of the free parameter β ought to be at any given collision frequency. We scanned this parameter and show the results for $\beta = 0$ and $\beta = -0.65$, the latter bringing the damping rates closer to those of the full FPO. But it is apparent that the wrong choice of β can also result in significant deviation from the FPO.

Also shown in figure 5(right) are the damping rates obtained when using the LBO-EM and the LBO-ET. Despite having a different model for u_{sr} and $v_{t,sr}$, LBO-EM has the same collision frequency ($\nu_{ei}^M = \nu_{ei}^G(\beta = 0)$) and gives the same damping rates as the LBO-G with $\beta = 0$ (top blue and dashed purple lines). The LBO-ET on the other hand

has a collision frequency that is smaller by the mass ratio ($\nu_{ei}^T = m_e \nu_{ei}^M / (m_e + m_i) \simeq (m_e/m_i) \nu_{ei}^M$), and therefore is essentially equivalent to neglecting cross-species collisions for this problem; i.e. solid black and dotted green lines agree. If we were to run the simulation with the LBO-ET but the same value of ν_{ei} as the LBO-EM then we would simply obtain the same results as if we had used the LBO-EM.

4.3. Velocity and temperature relaxation

As a final benchmark of the multispecies LBO algorithms and solvers we employ the gyroaveraged LBO to model the relaxation of a deuterium plasma to thermal equilibrium. We employ identical conditions, as best as we can tell, to those used in a benchmark of the FPO in the XGC code (Hager *et al.* 2016). The same test was recently performed with a finite-volume implementation of the LBO-ET and LBO-EM in GENE-X Ulbl *et al.* (2021). This means that the initial distribution functions are described by the bi-Maxwellians:

$$f_s(v_{\parallel}, \mu, t=0) = \frac{n_0}{\alpha (2\pi v_{t,s}^2)^{3/2}} \exp \left[-\frac{(v_{\parallel} - u_{\parallel s})^2 + 2\mu B / (m_s \alpha)}{2v_{t,s}^2} \right] \quad (4.8)$$

where $B = 1$ T, $v_{t,s} = \sqrt{T_{s0}/m_s}$, $\alpha = 1.3$, $u_{\parallel i} = 50(m_e/m_i)v_{t,i}$, $u_{\parallel e} = 0.5\sqrt{m_e/m_i}v_{t,s}$, $T_{i0} = 200$ eV and $T_{e0} = 300$ eV. Note that these reference temperatures are slightly different than the true initial temperatures $T_i(t=0) = 240$ eV and $T_e(t=0) = 360$ eV given by $T_s = (2T_{\perp s} + T_{\parallel s})/3$. For this test we once again neglect the collisionless terms and use a collision frequency that depends on time, i.e. $\nu_{sr} = \nu_{sr}(T_s(t), T_r(t))$. The phase space $[-2, 2] \times [-5v_{t,s}, 5v_{t,s}] \times [0, m_s(5v_{t,s})^2/(2B)]$ is meshed with 1×16^2 cells and dynamic fields are expanded in a piecewise linear ($p = 1$) basis. This resolution and velocity-space extents were confirmed as sufficient by convergence tests.

Figure 6 provides the time evolution of the parallel and perpendicular temperatures for the LBO-G ($\beta = 0$), LBO-EM and LBO-ET operators compared to the previously reported FPO results[†] (Hager *et al.* 2016). The first event is the isotropization of the electrons followed by the isotropization of the ions, happening on the ν_{ss}^{-1} time scale. We used

$$\nu_{ss} = \frac{1}{\sqrt{2}} \frac{q_s^4 n_s \log \Lambda_{ss}}{3 (2\pi)^{3/2} \epsilon_0^2 m_s^2 v_{t,s}^3}, \quad (4.9)$$

for the like-species scattering rate. Note that the LBO-G and LBO-EM exhibit a delayed isotropization time compared to the FPO's, an observation that Pezzi *et al.* (2015) had also made while comparing the self-species Dougherty operator to the FPO (in Landau form). Later, on the ν_{ie}^{-1} time scale we see the electrons and ions come into thermal equilibrium with each other, a process that is better described by both the LBO-G and the LBO-ET operators since, after all, the LBO-EM made no attempt at matching the FPO thermal relaxation rates. The time-axis on these plots has been normalized to the isotropization rate (Huba 2013)

$$\nu_T^i = \frac{2\sqrt{\pi} q_i^4 n_i \log \Lambda_{ii}}{(4\pi\epsilon_0)^2 m_i^2 v_{t,i}^3} A^{-2} [-3 + (A+3) a_F], \quad (4.10)$$

where $v_{t,i}$ and $\log \Lambda_{ii}$ use the initial ion temperature (240 eV), and $A = T_{\perp i}/T_{\parallel i} - 1$ and $a_F = A^{-1/2} \tan^{-1}(A^{1/2})$ if $A > 0$ or $a_F = (-A)^{1/2} \tanh^{-1}(-A)^{1/2}$ if $A < 0$.

[†] Note that the FPO results here (and those in figure 7) have been shifted in time by $-\Delta t = 3.85783 \times 10^{-7}$ s compared to those in Hager *et al.* (2016), since that work shifted them by Δt in order to show the results with a logarithmic x -axis.

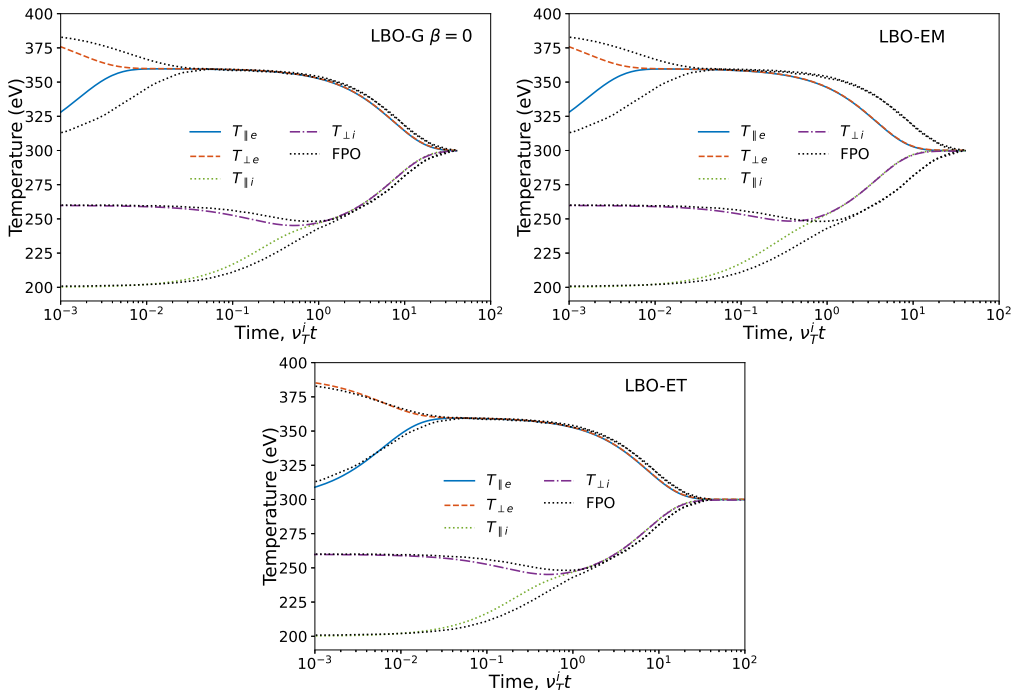


Figure 6: Isotropization and relaxation of temperatures as deuterium ions and electrons collide with themselves and each other, compared to the results from the full FPO (Hager *et al.* 2016). Top left: LBO-G with $\beta = 0$. Top right: LBO-EM. Bottom: LBO-ET.

We can also examine the velocity evolution as the plasma approaches an equilibrium as is done in figure 7. The first thing we notice is that the LBO-ET (green dash-dot with circles) grossly overestimates the time-scale on which the electron flow relaxes to the ion flow, which happens because the ions are so much more massive. By definition the LBO-ET did not attempt to match the momentum relaxation rate, and we see the result of that here. On the other hand, the LBO-G (solid blue) and LBO-EM (dashed orange with crosses) models do a better job of approximating the FPO results for the slowing down of electrons, since their formulation included matching the FPO’s momentum relaxation rates. There’s still a discrepancy, e.g. between solid blue and dashed orange lines, although we point out that the LBO-G and LBO-EM would appear to match the analytic result based on the flow relaxation frequency given by the friction force at large mass ratio (Hinton & Hazeltine 1976) (see figure 4 of Hager *et al.* (2016)).

5. Conclusion

This work presented three separate formulations of full- f nonlinear multispecies collisions based on the model Lenard-Bernstein or Dougherty operator (LBO), following the ideas Greene (1973) and Haack *et al.* (2017) employed for the BGK operator. This resulted in the LBO-G, LBO-EM and LBO-ET operators, each providing different formulas for the cross-species primitive moments $u_{sr,i}$ and $v_{t,sr}$ and collision frequency ν_{sr} . The LBO-G attempts to exactly match the thermal and momentum relaxation rates

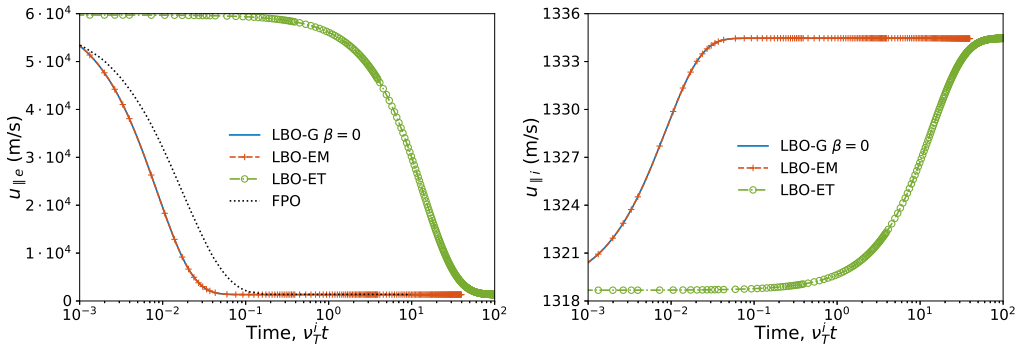


Figure 7: Relaxation of parallel flow speed as deuterium ions and electrons collide with themselves and each other. Electron flow speeds are compared to the results from the full FPO (dotted black, [Hager *et al.* \(2016\)](#)). Flow speeds when using the LBO-G ($\beta = 0$) are given in solid dark blue, results for the LBO-EM in dashed orange with crosses, and green dash-dot lines with circles represent results obtained with the LBO-ET.

of the Fokker-Planck operator (FPO), but it introduces a free parameter β . The LBO-EM only matches the FPO momentum relaxation rate, while the LBO-ET only tries to approximately match the FPO thermal relaxation rate. Gyroaveraged versions of this operators were also provided in this work, which may be used in long-wavelength gyrokinetic models. Compared to previous works, the multispecies LBO model presented here has the following advantages:

- It is suitable for arbitrary mass ratios.
- Some pathologies, such as negative cross-species temperatures (possible in the BGK operator of [Greene \(1973\)](#)), are avoided.
- It conserves energy and momentum exactly.
- It approximately reproduces the FPO's momentum and thermal relaxation rates.
- A proof of non-decreasing entropy (the H theorem) exists.

These multispecies LBO models may also be discretized for numerical implementation using a discontinuous Galerkin (DG) method in the spirit of [Hakim *et al.* \(2020\)](#) and [Francisquez *et al.* \(2020\)](#). We provided an algorithm for a DG discretization of such operators based on weak projections and the recovery of discontinuous derivatives across cell boundaries ([Hakim *et al.* 2020](#)). The primary focus of this work was, however, the computation of the cross-primitive moments $u_{sr,i}$ and $v_{t,sr}$ in a manner that results in an exactly conservative algorithm, i.e. capable of conserving particle, momentum and kinetic energy density independently of resolution. This property was accomplished by solving a weak system of equations consisting of the discrete equivalent of momentum and energy conservation, and in the case of the LBO-G, a discrete equivalent of the momentum and thermal relaxation rate constraints. Discrete conservation was also attained when piecewise-linear basis functions ($p = 1$) were used by carefully employing the projection of v^2 onto the basis (or v_{\parallel}^2 for the gyroaveraged operator).

Our tests indicate that the implementation in `Gkeyll` exhibits this exact conservation feature, for all the velocity dimensions and polynomial orders tested. Exact conservation was also confirmed in `Gkeyll`'s gyroaveraged solver for one and two velocity dimensions. In addition we combined the LBO solver with `Gkeyll`'s Vlasov-Maxwell solver and examined the impact that LBO cross-species collisions has on the Landau damping rates of electron Langmuir waves. Due to the definition of the LBO-ET collision frequency, such operator gave no improvements over using self-species collisions only, while the

LBO-G and LBO-EM gave slightly more accurate descriptions of this phenomenon. The LBO-G can be made to agree more with the FPO by choosing a different value of β , but we have not presented a first-principles model for that free parameter yet. Despite this unspecified parameter, the LBO-G operator has been in use by Gkeyll's Vlasov and gyrokinetic solvers for quite some time now. For example, recent Vlasov-Maxwell simulations using this operator showed the inhibition of magnetic dynamo due to Landau damping (Pusztai *et al.* 2020). Nevertheless, this β parameter will be the focus of follow up work.

Lastly, we benchmarked the gyroaveraged multispecies LBO by simulating a system in which ions and electrons are anisotropic, drifting relative to each other, and out of thermal equilibrium. The LBO-EM and LBO-ET each do better at approximating the FPO's velocity and temperature evolution, as their formulation would predict. The LBO-G is perhaps the best choice here, since it does well at matching the temperature evolution and provides the same level of accuracy when it comes to the velocity relaxation as the LBO-EM.

Acknowledgements

We express our gratitude towards Rogerio Jorge and Robert Hager for clarifying how the FPO results were obtained, as well as our gratitude for the other members of the Gkeyll team who aided this work. We used the Stellar cluster at Princeton University and the Cori cluster at the National Energy Research Scientific Computing Center (NERSC), a U.S. Department of Energy Office of Science User Facility. M.F., A.H. and G.W.H. were supported by the Partnership for Multiscale Gyrokinetic Turbulence (MGK) and the High-Fidelity Boundary Plasma Simulation (HBPS) projects, part of the U.S. Department of Energy (DOE) Scientific Discovery Through Advanced Computing (SciDAC) program, and the DOE's ARPA-E BETHE program, via DOE contract DE-AC02-09CH11466 for the Princeton Plasma Physics Laboratory. J.J. was supported by a NSF Atmospheric and Geospace Science Postdoctoral Fellowship (Grant No. AGS-2019828). M.F., as well as D.R.E., was also supported by the Partnership for Multiscale Gyrokinetic Turbulence (MGK) (subaward No. UTA18-000276 to M.I.T. under U.S. DOE Contract DE-SC0018429).

Declaration of Interests

The authors report no conflict of interest.

Data availability statement

The data that support the findings of this study are openly available in Zenodo at <https://doi.org/10.5281/zenodo.6350748>.

Appendix A. Getting Gkeyll and reproducing results

Readers may reproduce our results and also use Gkeyll for their applications. The code and input files used here are available online. Full installation instructions for Gkeyll are provided on the Gkeyll website Gkeyll (2020). The code can be installed on Unix-like operating systems (including Mac OS and Windows using the Windows Subsystem for Linux) either by installing the pre-built binaries using the conda package manager (<https://www.anaconda.com>) or building the code via

sources. The input files used here are under version control and can be found at https://github.com/ammahakim/gkyl-paper-inp/tree/master/2021_JPP_crossLBO.

Appendix B. H -theorem proof

In this section we show that the improved interspecies Dougherty collisions do not decrease total entropy given the cross-species primitive moments for collisions between species s and species r (equations 2.8-2.9). The rate of change of the entropy \mathcal{S} can be written as

$$\begin{aligned} \frac{\partial \mathcal{S}}{\partial t} &= -\frac{\partial}{\partial t} \sum_s \int d^{d_v} v f_s \ln f_s \\ &= -\sum_s \int d^{d_v} v \frac{\partial f_s}{\partial t} (\ln f_s + 1), \\ &= -\sum_s \int d^{d_v} v \nu_{sr} (\nabla_v \cdot \mathbf{J}_{sr}) (\ln f_s + 1), \end{aligned} \quad (\text{B1})$$

where $\mathbf{J}_{sr} = (\mathbf{v} - \mathbf{u}_{sr}) f_s + v_{t,sr}^2 \nabla_v f_s$. Integrate equation B1 by parts and use the fact that $f_s \rightarrow 0$ faster than any polynomial or logarithmic singularity. In the interest of simplicity we adopt the notation $\int_{d_v} = \int d^{d_v} v$, then the time rate of change $\dot{\mathcal{S}}$ becomes

$$\begin{aligned} \dot{\mathcal{S}} &= \sum_s \int_{d_v} \nu_{sr} \mathbf{J}_{sr} \nabla_v (\ln f_s + 1) \\ &= \sum_s \int_{d_v} \nu_{sr} [(\mathbf{v} - \mathbf{u}_{sr}) f_s + v_{t,sr}^2 \nabla_v f_s] \cdot \nabla_v \ln f_s, \\ &= \sum_s \int_{d_v} \nu_{sr} [(\mathbf{v} - \mathbf{u}_{sr}) \cdot \nabla_v f_s + v_{t,sr}^2 \nabla_v f_s \cdot \nabla_v \ln f_s]. \end{aligned} \quad (\text{B2})$$

The first term can be integrated again so that upon discarding the surface term, and adopting the notation $\dot{\mathcal{N}}_{sr} = \nu_{sr} d_v n_s$ and $\dot{\mathcal{T}}_{sr} = \nu_{sr} v_{t,sr}^2$, one obtains

$$\dot{\mathcal{S}} = \sum_s \left(-\dot{\mathcal{N}}_{sr} + \dot{\mathcal{T}}_{sr} \int_{d_v} \nabla_v f_s \cdot \nabla_v \ln f_s \right). \quad (\text{B3})$$

At this point we can ask what is the distribution function that minimizes $\dot{\mathcal{S}}$. Given a set of primitive moments ($u_{sr,i}$, $v_{t,sr}$, and also $u_{s,i}$, $v_{t,s}$) and the virtual displacement $\delta f_s = f_s - f_{s0}$, the response of the functional in equation B3 is

$$\begin{aligned} \delta \dot{\mathcal{S}} &= \sum_s \dot{\mathcal{T}}_{sr} \int_{d_v} \left[\delta \left(\frac{1}{f_s} \right) |\nabla_v f_{s0}|^2 + \frac{1}{f_{s0}} \delta |\nabla_v f_s|^2 \right], \\ &\approx \sum_s \dot{\mathcal{T}}_{sr} \int_{d_v} \frac{1}{f_{s0}} \left(-\frac{\delta f_s}{f_{s0}} |\nabla_v f_{s0}|^2 + 2 \nabla_v f_{s0} \cdot \nabla_v \delta f_s \right), \\ &= \sum_s \dot{\mathcal{T}}_{sr} \int_{d_v} \left\{ \frac{1}{f_{s0}} \left(-\frac{\delta f_s}{f_{s0}} \right) |\nabla_v f_{s0}|^2 + 2 \left[\nabla_v \cdot \frac{\delta f_s}{f_{s0}} \nabla_v f_{s0} - \delta f_s \nabla_v \cdot \frac{1}{f_{s0}} \nabla_v f_{s0} \right] \right\}. \end{aligned} \quad (\text{B4})$$

The second term vanishes since $\delta f_s \rightarrow \pm\infty$ as $v_i \rightarrow \pm\infty$. Thus at an extremum

$$\delta \dot{\mathcal{S}} = \sum_s \dot{\mathcal{T}}_{sr} \int_{d_v} \left[-\frac{1}{f_{s0}^2} |\nabla_v f_{s0}|^2 - 2 \nabla_v \cdot \frac{1}{f_{s0}} \nabla_v f_{s0} \right] \delta f_s \quad (\text{B5})$$

must vanish, and since equation B 3 has no upper bound this extremum must be a minimum. At this point we can impose the conditions

$$\int_{d_v} \delta f_s = 0, \quad (\text{B 6})$$

$$\int_{d_v} m_s \mathbf{v} \delta f_s = 0, \quad (\text{B 7})$$

$$\int_{d_v} \frac{1}{2} m_s v^2 \delta f_s = 0, \quad (\text{B 8})$$

requiring the virtual displacement to not alter the moments of the solution (but does not mean that the moments are constant in time). From equations B 5-B 8 we can deduce that for equation B 5 to vanish for all displacements δf_s it must be that

$$|\nabla_{\mathbf{v}} \ln f_{s0}|^2 + 2\nabla_{\mathbf{v}}^2 \ln f_{s0} = a + \mathbf{b} \cdot \mathbf{v} + cv^2, \quad (\text{B 9})$$

where a , \mathbf{b} and c are constants. We can re-write this equation as

$$h(t, \mathbf{x}, \mathbf{v})^2 + 2\nabla_{\mathbf{v}} \cdot \mathbf{h}(t, \mathbf{x}, \mathbf{v}) = a + \mathbf{b} \cdot \mathbf{v} + cv^2, \quad (\text{B 10})$$

where $\mathbf{h}(t, \mathbf{x}, \mathbf{v}) = \nabla_{\mathbf{v}} \ln f_{s0}$. We claim that the solution to this nonlinear inhomogeneous equation is

$$\mathbf{h}(t, \mathbf{x}, \mathbf{v}) = \mathbf{h}_0 + h_1 \mathbf{v}, \quad (\text{B 11})$$

with \mathbf{h}_0 and h_1 yet undetermined constants. Check by substituting equation B 11 into equation B 10:

$$h(t, \mathbf{x}, \mathbf{v})^2 + 2\nabla_{\mathbf{v}} \cdot \mathbf{h}(t, \mathbf{x}, \mathbf{v}) = h_0^2 + 2h_1 \mathbf{h}_0 \cdot \mathbf{v} + h_1^2 v^2 + 2\nabla_{\mathbf{v}} \cdot (\mathbf{h}_0 + h_1 \mathbf{v}), \quad (\text{B 12})$$

which has the same form as the right side of equation B 10 with $a = h_0^2 + 2d_v h_1$, $\mathbf{b} = 2h_1 \mathbf{h}_0$ and $c = h_1^2$. Going back to the definition of $\mathbf{h}(t, x_i, v_i)$, we can arrive at

$$\begin{aligned} \ln f_{s0} &= g_0 + \mathbf{h}_0 \cdot \mathbf{v} + \frac{1}{2} h_1 v^2, \\ \Rightarrow f_{s0} &= A \exp\left(\mathbf{h}_0 \cdot \mathbf{v} + \frac{1}{2} h_1 v^2\right). \end{aligned} \quad (\text{B 13})$$

We can now explore whether our minimized $\dot{\mathcal{S}}$ falls below zero. For this we rewrite equation B 3 making use of vanishing total derivatives

$$\min(\dot{\mathcal{S}}) = \sum_s \left(-\dot{\mathcal{N}}_{sr} - \dot{\mathcal{T}}_{sr} \int_{d_v} f_{s0} \nabla_{\mathbf{v}} \cdot \frac{1}{f_{s0}} \nabla_{\mathbf{v}} f_{s0} \right), \quad (\text{B 14})$$

and, from equation B 9,

$$f_{s0} \nabla_{\mathbf{v}} \cdot \frac{1}{f_{s0}} \nabla_{\mathbf{v}} f_{s0} = \frac{a + \mathbf{b} \cdot \mathbf{v} + cv^2}{2} f_{s0} - \frac{1}{2f_{s0}} |\nabla_{\mathbf{v}} f_{s0}|^2. \quad (\text{B 15})$$

Putting these two equations together we have:

$$\min(\dot{\mathcal{S}}) = \sum_s \left[-\dot{\mathcal{N}}_{sr} - \frac{1}{2} \dot{\mathcal{T}}_{sr} \int_{d_v} \left(a + \mathbf{b} \cdot \mathbf{v} + cv^2 - |\nabla_{\mathbf{v}} \ln f_{s0}|^2 \right) f_{s0} \right]. \quad (\text{B 16})$$

Take the derivative of equation B 13 and insert it into equation B 16 to obtain

$$\min(\dot{\mathcal{S}}) = \sum_s \left[-\dot{\mathcal{N}}_{sr} - \frac{1}{2} \dot{\mathcal{T}}_{sr} \int_{d_v} \left(a + \mathbf{b} \cdot \mathbf{v} + cv^2 - |\mathbf{h}_0 + h_1 \mathbf{v}|^2 \right) f_{s0} \right]. \quad (\text{B 17})$$

Employing the definitions of a , b_i and c above this becomes

$$\min(\dot{\mathcal{S}}) = \sum_s \left(-\dot{N}_{sr} - d_v h_1 \dot{T}_{sr} \int_{d_v} f_{s0} \right). \quad (\text{B } 18)$$

If we require that the zeroth moment of f_{s0} equals n_s , we find that

$$f_{s0} = n_s \left(-\frac{h_1}{2\pi} \right)^{d_v/2} \exp \left[\frac{(\mathbf{h}_0 + h_1 \mathbf{v})^2}{2h_1} \right]. \quad (\text{B } 19)$$

Identify h_1 with $-v_{t,s}^{-2}$ such that the minimizing function becomes

$$f_{s0} = \frac{n_s}{(2\pi v_{t,s}^2)^{d_v/2}} \exp \left[-\frac{(v_{t,s}^2 \mathbf{h}_0 - \mathbf{v})^2}{2v_{t,s}^2} \right], \quad (\text{B } 20)$$

and by taking the first moment of this distribution it would become clear that $v_{t,s}^2 \mathbf{h}_0 = \mathbf{u}_s$. The minimizing distribution is thus a Maxwellian with number density n_s , mean flow velocity \mathbf{u}_s and thermal speed $v_{t,s}$. Since we have found a single distribution that minimizes $\dot{\mathcal{S}}$ then the minimum given below must be global.

One can show that if the two colliding distributions are Maxwellian, that the total entropy does not decrease. We can check this here by going back to equation B 18, and find that the minimum entropy rate of change is

$$\min(\dot{\mathcal{S}}) = -d_v \sum_s n_s \nu_{sr} \left(1 - \frac{v_{t,sr}^2}{v_{t,s}^2} \right). \quad (\text{B } 21)$$

At this point one must substitute the definition for the cross-species thermal speed in equation 2.9 to yield

$$\begin{aligned} \min(\dot{\mathcal{S}}) &= d_v \sum_s \frac{n_s \nu_{sr}}{v_{t,s}^2} \frac{\delta_s}{2} \frac{1 + \beta}{1 + \frac{m_r}{m_s}} \left[\frac{m_r}{m_s} v_{t,r}^2 + \frac{1}{d_v} \frac{m_r}{m_s} (\mathbf{u}_s - \mathbf{u}_r)^2 - v_{t,s}^2 \right], \\ &= d_v \frac{m_s n_s \nu_{sr}}{v_{t,s}^2} \frac{\delta_s}{2} \frac{1 + \beta}{m_s + m_r} \sum_s \left[\frac{T_r}{T_s} + \frac{1}{d_v} \frac{m_r}{m_s} \frac{(\mathbf{u}_s - \mathbf{u}_r)^2}{v_{t,s}^2} - 1 \right], \\ &= d_v \frac{m_s n_s \nu_{sr}}{v_{t,s}^2} \frac{\delta_s}{2} \frac{1 + \beta}{m_s + m_r} \left[\frac{(T_r - T_s)^2}{T_s T_r} + \frac{1}{d_v} \left(\frac{m_r}{m_s} \frac{1}{v_{t,s}^2} + \frac{m_s}{m_r} \frac{1}{v_{t,r}^2} \right) (\mathbf{u}_s - \mathbf{u}_r)^2 \right] \geq 0. \end{aligned} \quad (\text{B } 22)$$

and thus the entropy cannot decrease and the H -theorem of this nonlinear full- f multi-species collision model is guaranteed.

Appendix C. Energy conservation with piecewise linear basis

C.1. Cartesian $p=1$ energy conservation

The derivation of a constraint on the operator to conserve energy in section 3.2 relied on v^2 belonging to the space span by the basis set. For piecewise linear basis ($p = 1$) that is not the case, so instead we can guarantee that the algorithm preserves the projection of the energy onto the basis. We use the notation and strategy first outlined in Hakim *et al.* (2020) for self-species collisions; \bar{v}^2 is the projection of v^2 onto the basis. For the energy to be conserved the left side of equation 3.1 has to be zero after making the substitution

$\psi_\ell = m_s \overline{v^2}/2$, summing over species and over all cells. Those steps lead to the relation

$$\sum_j \int_{x_{i-1/2}}^{x_{i+1/2}} \left\{ \frac{m_s}{2} \nu_{sr} \left[\left(\overline{v^2} G_s - \frac{\partial \overline{v^2}}{\partial v} v_{t,sr}^2 \hat{f}_s \right) \Big|_{v_{j-1/2}}^{v_{j+1/2}} - \int_{v_{j-1/2}}^{v_{j+1/2}} \frac{\partial \overline{v^2}}{\partial v} (v - u_{sr}) f_s dv \right] + \frac{m_s}{2} \nu_{rs} \left[\left(\overline{v^2} G_r - \frac{\partial \overline{v^2}}{\partial v} v_{t,rs}^2 \hat{f}_r \right) \Big|_{v_{j-1/2}}^{v_{j+1/2}} - \int_{v_{j-1/2}}^{v_{j+1/2}} \frac{\partial \overline{v^2}}{\partial v} (v - u_{rs}) f_r dv \right] \right\} dx = 0, \quad (\text{C1})$$

where we used $\partial^2 \overline{v^2} / \partial v^2 = 0$. Next we use the fact that (Hakim *et al.* 2020)

$$\frac{1}{2} \frac{\partial \overline{v^2}}{\partial v} = \check{v}_j = \frac{v_{j-1/2} + v_{j+1/2}}{2} \quad (\text{C2})$$

(the cell center) and the continuity of $\overline{v^2} G_s$ as well at the zero flux boundary conditions, to turn equation C1 into

$$\int_{x_{i-1/2}}^{x_{i+1/2}} \sum_j \left\{ m_s \nu_{sr} \left[-\check{v}_j v_{t,sr}^2 \hat{f}_s \Big|_{v_{j-1/2}}^{v_{j+1/2}} - \int_{v_{j-1/2}}^{v_{j+1/2}} \check{v}_j (v - u_{sr}) f_s dv \right] + m_s \nu_{rs} \left[-\check{v}_j v_{t,rs}^2 \hat{f}_r \Big|_{v_{j-1/2}}^{v_{j+1/2}} - \int_{v_{j-1/2}}^{v_{j+1/2}} \check{v}_j (v - u_{rs}) f_r dv \right] \right\} dx = 0. \quad (\text{C3})$$

Carrying out the velocity integrals this equation becomes

$$\int_{x_{i-1/2}}^{x_{i+1/2}} \left\{ m_s \nu_{sr} \left[-v_{t,sr}^2 \left(\check{v}_j f_s(v_{j\pm 1/2}) \Big|_{j_{\min}}^{j_{\max}} - M_{0,s}^* \right) - (M_{2,s}^* - u_{sr} M_{1,s}^*) \right] + m_s \nu_{rs} \left[-v_{t,rs}^2 \left(\check{v}_j f_r(v_{j\pm 1/2}) \Big|_{j_{\min}}^{j_{\max}} - M_{0,r}^* \right) - (M_{2,r}^* - u_{rs} M_{1,r}^*) \right] \right\} dx = 0, \quad (\text{C4})$$

where the \pm sign is used when evaluating at j_{\max}/j_{\min} and we have introduced the star moments

$$\begin{aligned} M_{0,s}^* &= \sum_{j=1}^{N_v-1} (\check{v}_{j+1} - \check{v}_j) \hat{f}_{s,j+1/2}, \\ M_{1,s}^* &= \sum_{j=1}^{N_v} \int_{v_{j-1/2}}^{v_{j+1/2}} \check{v}_j f_s dv, \\ M_{2,s}^* &= \sum_{j=1}^{N_v} \int_{v_{j-1/2}}^{v_{j+1/2}} \check{v}_j v f_s dv. \end{aligned} \quad (\text{C5})$$

Therefore our DG scheme will conserve energy if we enforce the following weak constraint

$$\begin{aligned} & m_s \nu_{sr} \left[u_{sr} M_{1,s}^* + v_{t,sr}^2 \left(M_{0,s}^* - \check{v}_j f_s(v_{j\pm 1/2}) \Big|_{j_{\min}}^{j_{\max}} \right) \right] \\ & + m_r \nu_{rs} \left[u_{rs} M_{1,r}^* + v_{t,rs}^2 \left(M_{0,r}^* - \check{v}_j f_r(v_{j\pm 1/2}) \Big|_{j_{\min}}^{j_{\max}} \right) \right] \doteq m_s \nu_{sr} M_{2,s}^* + m_r \nu_{rs} M_{2,r}^*. \end{aligned} \quad (\text{C6})$$

In order to formulate an energy-conserving LBO-G with $p = 1$ we also need to re-examine the thermal relaxation rate of the discrete operator, equation 3.12. If we instead substitute $\psi_\ell = m_s \overline{(v - u_s)^2} / 2 = m_s (\overline{v^2} - 2v u_s + u_s^2) / 2$ into equation 3.1 and sum over

velocity-space cells we get

$$\begin{aligned} \sum_j \int_{K_{i,j}} \frac{m_s \overline{(v - u_s)^2}}{2} \left(\frac{df_s}{dt} \right)_c dx dv = & - \int_{x_{i-1/2}}^{x_{i+1/2}} m_s \nu_{sr} \sum_j \left[(\check{v}_j - u_s) v_{t,sr}^2 \hat{f}_s \Big|_{v_{j-1/2}}^{v_{j+1/2}} \right. \\ & \left. + \int_{v_{j-1/2}}^{v_{j+1/2}} (\check{v}_j - u_s) (v - u_{sr}) f_s dv \right] dx, \end{aligned} \quad (\text{C7})$$

having used the continuity of $\overline{(v - u_s)^2} G_s$, its boundary conditions, equation C2 and $\partial^2 v^2 / \partial v^2 = 0$. Carry out the velocity-space integrals on the right as well as the sum over j in order to land at

$$\begin{aligned} \sum_j \int_{K_{i,j}} \frac{m_s \overline{(v - u_s)^2}}{2} \left(\frac{df_s}{dt} \right)_c dx dv \\ = \int_{x_{i-1/2}}^{x_{i+1/2}} m_s \nu_{sr} \left[v_{t,sr}^2 \left(M_{0,s}^* - \check{v}_j f_s(v_{j\pm 1/2}) \Big|_{j_{\min}}^{j_{\max}} + u_s \hat{f}_s \Big|_{v_{j_{\min}-1/2}}^{v_{j_{\max}+1/2}} \right) \right. \\ \left. + u_{sr} (M_{1,s}^* - u_s M_{0,s}) - (M_{2,s}^* - u_s M_{1,s}) \right] dx. \end{aligned} \quad (\text{C8})$$

Therefore when using $p = 1$ bases we enforce the equality of the relaxation rates with

$$\begin{aligned} m_s \nu_{sr} \left[u_{sr} (M_{1,s}^* - u_s M_{0,s}) + v_{t,sr}^2 \left(M_{0,s}^* - \check{v}_j f_s(v_{j\pm 1/2}) \Big|_{j_{\min}}^{j_{\max}} + u_s \hat{f}_s \Big|_{v_{j_{\min}-1/2}}^{v_{j_{\max}+1/2}} \right) \right. \\ - m_r \nu_{rs} \left[u_{rs} (M_{1,r}^* - u_r M_{0,r}) + v_{t,rs}^2 \left(M_{0,r}^* - \check{v}_j f_r(v_{j\pm 1/2}) \Big|_{j_{\min}}^{j_{\max}} + u_r \hat{f}_r \Big|_{v_{j_{\min}-1/2}}^{v_{j_{\max}+1/2}} \right) \right. \\ \left. \doteq m_s \nu_{sr} (M_{2,s}^* - u_s M_{1,s}) - m_r \nu_{rs} (M_{2,r}^* - u_r M_{1,r}) \right. \\ \left. + \frac{\alpha_E}{M_{0,s} M_{0,r}} [m_r M_{0,s} (M_{2,r} - u_{r,i} M_{1,i,r}) - m_s M_{0,r} (M_{2,s} - u_{s,i} M_{1,i,s}) \right. \\ \left. + \frac{m_r - m_s}{2} (u_{s,i} - u_{r,i}) (M_{0,r} M_{1,i,s} - M_{0,s} M_{1,i,r}) \right]. \end{aligned} \quad (\text{C9})$$

C.2. Gyroaveraged $p=1$ energy conservation

Energy conservation with $p = 1$ basis functions is also possible with the gyroaveraged operator in equation 2.35. The discretization and calculation of the cross-primitive moments follows in the vein of that explained in section 3.4.1, although this time we must consider the projection of the v_{\parallel}^2 onto the $p = 1$ as was done for the non-gyroaveraged operator in the previous section. Substituting $\psi_{\ell} = m_s \overline{v_{\parallel}^2} / 2$ into the weak form of the gyroaveraged collision operator, summing over velocity-space cells and species we obtain the following constraint

$$\begin{aligned} m_s \nu_{sr} \left\{ u_{\parallel sr} M_{1\parallel,s}^* + v_{t,sr}^2 \left[M_{0,s}^* + 2M_{0,s} - \frac{2\pi}{m_s} \left(\int \check{v}_{\parallel j} f_s(v_{\parallel j\pm 1/2}) \Big|_{j_{\min}}^{j_{\max}} d\mu \right. \right. \right. \\ \left. \left. + 2 \int \mu f_s \Big|_{\mu_{\min}}^{\mu_{\max}} dv_{\parallel} \right) \right] \right\} \\ + m_r \nu_{rs} \left\{ u_{rs} M_{1\parallel,r}^* + v_{t,rs}^2 \left[M_{0,r}^* + 2M_{0,r} - \frac{2\pi}{m_r} \left(\int \check{v}_{\parallel j} f_r(v_{\parallel j\pm 1/2}) \Big|_{j_{\min}}^{j_{\max}} d\mu \right. \right. \right. \\ \left. \left. + 2 \int \mu f_r \Big|_{\mu_{\min}}^{\mu_{\max}} dv_{\parallel} \right) \right] \right\} \doteq m_s \nu_{sr} M_{2,s}^* + m_r \nu_{rs} M_{2,r}^*. \end{aligned} \quad (\text{C10})$$

In addition to energy conservation the gyroaveraged LBO-G requires the discrete thermal relaxation rate of the operator, which we must re-calculate assuming $p = 1$ basis functions. Multiplying the discrete gyroaveraged LBO by $\psi_\ell = m_s(v - u_{\parallel s})^2/2 + \mu B$, integrating over phase-space and summing over velocity space cells we obtain the following discrete relaxation rate:

$$\begin{aligned}
& \sum_{j,k} \int_{K_{i,j,k}} \left[\frac{m_s}{2} \overline{(v_{\parallel} - u_{\parallel s})^2} + \mu B \right] \left(\frac{\partial f_s}{\partial t} \right)_c dx dv_{\parallel} d\mu = \\
& \nu_{sr} \sum_{j,k} \left(\int_{\mu_{k-1/2}}^{\mu_{k+1/2}} \left\{ \left[\frac{m_s}{2} \overline{(v_{\parallel} - u_{\parallel s})^2} + \mu B \right] G_{v_{\parallel s}} - m_s (\check{v}_{\parallel j} - u_{\parallel s}) v_{t,sr}^2 \hat{f}_s \right\} \Big|_{v_{\parallel j-1/2}}^{v_{\parallel j+1/2}} d\mu \right. \\
& + \int_{v_{\parallel j-1/2}}^{v_{\parallel j+1/2}} \left\{ \left[\frac{m_s}{2} \overline{(v_{\parallel} - u_{\parallel s})^2} + \mu B \right] G_{\mu s} - 2\mu m_s v_{t,sr}^2 \hat{f}_s \right\} \Big|_{\mu_{k-1/2}}^{\mu_{k+1/2}} dv_{\parallel} \\
& \left. - \int_{K_{i,j,k}} [m_s (\check{v}_{\parallel j} - u_{\parallel s}) (v_{\parallel} - u_{\parallel sr}) f_s + B 2\mu f_s - 2m_s v_{t,sr}^2 f_s] dx dv_{\parallel} d\mu \right), \tag{C 11}
\end{aligned}$$

where $j(k)$ labels the cell along $v_{\parallel}(\mu)$, and we used the fact that $\overline{m_s(v - u_{\parallel s})^2/2 + \mu B}$ is linear in v_{\parallel} and that its v_{\parallel} derivative is $m_s(\check{v}_{\parallel j} - u_{\parallel s})$. In equation C 11 the $G_{v_{\parallel s}}$ and $G_{\mu s}$ are numerical fluxes (Francisquez *et al.* 2020). Doing the velocity-space integrals, carrying out the sums over velocity space cells, using the continuity of $G_{v_{\parallel s}}$, $G_{\mu s}$ and \hat{f}_s and the zero-flux BCs one obtains

$$\begin{aligned}
& \sum_{j,k} \int_{K_{i,j,k}} \left[\frac{m_s}{2} \overline{(v_{\parallel} - u_{\parallel s})^2} + \mu B \right] \left(\frac{\partial f_s}{\partial t} \right)_c dx dv_{\parallel} d\mu = \\
& m_s \nu_{sr} \int_{x_{i-1/2}}^{x_{i+1/2}} \left\{ v_{t,sr}^2 \left[2M_{0,s} + M_{0,s}^* - \frac{2\pi}{m_s} \left(\sum_k \int_{\mu_{k-1/2}}^{\mu_{k+1/2}} \check{v}_{\parallel j} f_s(v_{\parallel j \pm 1/2}) \Big|_{j_{\min}}^{j_{\max}} d\mu \right. \right. \right. \\
& \left. \left. + 2 \sum_j \int_{v_{\parallel j-1/2}}^{v_{\parallel j+1/2}} \mu f_s \Big|_{\mu_{\min}}^{\mu_{\max}} dv_{\parallel} \right) \right] + u_{\parallel sr} (M_{1\parallel,s}^* - u_{\parallel s} M_{0,s}) - (M_{2,s}^* - u_{\parallel s} M_{1\parallel,s}) \left. \right\} dx. \tag{C 12}
\end{aligned}$$

Using this equation we can enforce the equality between the discrete thermal relaxation

rates via

$$\begin{aligned}
& m_s \nu_{sr} \left\{ u_{\parallel sr} \left(M_{1\parallel, s}^* - u_{\parallel s} M_{0, s} \right) + v_{t, sr}^2 \left[2M_{0, s} + M_{0, s}^* \right. \right. \\
& \quad \left. \left. - \frac{2\pi}{m_s} \left(\sum_k \int_{\mu_{k-1/2}}^{\mu_{k+1/2}} \check{v}_{\parallel j} f_s(v_{\parallel j \pm 1/2}) \right) \Big|_{j_{\min}}^{j_{\max}} d\mu + 2 \sum_j \int_{v_{\parallel j-1/2}}^{v_{\parallel j+1/2}} \mu f_s \Big|_{\mu_{\min}}^{\mu_{\max}} dv_{\parallel} \right] \right\} \\
& - m_r \nu_{rs} \left\{ u_{\parallel rs} \left(M_{1\parallel, r}^* - u_{\parallel r} M_{0, r} \right) + v_{t, rs}^2 \left[2M_{0, r} + M_{0, r}^* \right. \right. \\
& \quad \left. \left. - \frac{2\pi}{m_r} \left(\sum_k \int_{\mu_{k-1/2}}^{\mu_{k+1/2}} \check{v}_{\parallel j} f_r(v_{\parallel j \pm 1/2}) \right) \Big|_{j_{\min}}^{j_{\max}} d\mu + 2 \sum_j \int_{v_{\parallel j-1/2}}^{v_{\parallel j+1/2}} \mu f_r \Big|_{\mu_{\min}}^{\mu_{\max}} dv_{\parallel} \right] \right\} \quad (C13) \\
& \doteq m_s \nu_{sr} \left(M_{2, s}^* - u_{\parallel s} M_{1\parallel, s} \right) - m_r \nu_{rs} \left(M_{2, r}^* - u_{\parallel r} M_{1\parallel, r} \right) \\
& + \frac{\alpha E}{M_{0, s} M_{0, r}} \left[m_r M_{0, s} \left(M_{2, r} - u_{\parallel r} M_{1\parallel, r} \right) - m_s M_{0, r} \left(M_{2, s} - u_{\parallel s} M_{1\parallel, s} \right) \right. \\
& \left. + \frac{m_r - m_s}{2} \left(u_{\parallel s} - u_{\parallel r} \right) \left(M_{0, r} M_{1\parallel, s} - M_{0, s} M_{1\parallel, r} \right) \right].
\end{aligned}$$

REFERENCES

- ABEL, I. G., BARNES, M., COWLEY, S. C., DORLAND, W. & SCHEKOCHIHIN, A. A. 2008 Linearized model Fokker–Planck collision operators for gyrokinetic simulations. I. Theory. *Physics of Plasmas* **15** (12), 122509.
- ANDERSON, M. W. & O’NEIL, T. M. 2007 Eigenfunctions and eigenvalues of the Dougherty collision operator. *Physics of Plasmas* **14** (5), 052103.
- BHATNAGAR, P. L., GROSS, E. P. & KROOK, M. 1954 A Model for Collision Processes in Gases. I. Small Amplitude Processes in Charged and Neutral One-Component Systems. *Physical Review* **94**, 511–525.
- COCKBURN, B. & SHU, C.-W. 1998 The local discontinuous Galerkin method for time-dependent convection-diffusion systems. *SIAM Journal on Numerical Analysis* **35** (6), 2440–2463.
- DOUGHERTY, J. P. 1964 Model Fokker-Planck Equation for a Plasma and Its Solution. *The Physics of Fluids* **7** (11), 1788–1799.
- DOUGHERTY, J. P. & WATSON, S. R. 1967 Model Fokker-Planck Equations: Part 2. The equation for a multicomponent plasma. *Journal of Plasma Physics* **1** (3), 317–326.
- ESTÈVE, D., GARBET, X., SARAZIN, Y., GRANDGIRARD, V., CARTIER-MICHAUD, T., DIF-PRADALIER, G., GHENDRIH, P., LATU, G. & NORSCINI, C. 2015 A multi-species collisional operator for full-F gyrokinetics. *Physics of Plasmas* **22** (12), 122506.
- FRANCISQUEZ, M., BERNARD, T. N., MANDELL, N. R., HAMMETT, G. W. & HAKIM, A. 2020 Conservative discontinuous Galerkin scheme of a gyro-averaged Dougherty collision operator. *Nuclear Fusion* **60** (9), 096021.
- FREI, B.J., BALL, J., HOFFMANN, A.C.D., JORGE, R., RICCI, P. & STENGER, L. 2021 Development of advanced linearized gyrokinetic collision operators using a moment approach. *Journal of Plasma Physics* **87**, 905870501.
- GKEYLL 2020 The Gkeyll 2.0 Code: Documentation Home. <http://gkeyll.readthedocs.io>.
- GREENE, J. M. 1973 Improved Bhatnagar-Gross-Krook model of electron-ion collisions. *The Physics of Fluids* **16** (11), 2022–2023.
- HAACK, J. R., HAUCK, C. D. & MURILLO, M. S. 2017 A Conservative, Entropic Multispecies BGK Model. *Journal of Statistical Physics* **168** (4), 826–856.
- HAGER, R., YOON, E.S., KU, S., D’AZEVEDO, E.F., WORLEY, P.H. & CHANG, C.S. 2016 A fully non-linear multi-species fokker–planck–landau collision operator for simulation of fusion plasma. *Journal of Computational Physics* **315**, 644–660.
- HAKIM, A., FRANCISQUEZ, M., JUNO, J. & HAMMETT, G. W. 2020 Conservative discontinuous

- Galerkin schemes for nonlinear Dougherty-Fokker-Planck collision operators. *Journal of Plasma Physics* **86** (4), 905860403.
- HAKIM, A. & JUNO, J. 2020 Alias-free, matrix-free, and quadrature-free discontinuous galerkin algorithms for (plasma) kinetic equations. In *Proceedings of the International Conference for High Performance Computing, Networking, Storage and Analysis, SC '20* 73. IEEE Press.
- HESTHAVEN, J. S. & WARBURTON, T. 2007 *Nodal discontinuous Galerkin methods: algorithms, analysis, and applications*. Springer Science & Business Media.
- HINTON, F. L. & HAZELTINE, R. D. 1976 Theory of plasma transport in toroidal confinement systems. *Reviews of Modern Physics* **48**, 239–308.
- HIRVIJOKI, E., BRIZARD, A. J. & PFEFFERLÉ, D. 2017 Differential formulation of the gyrokinetic Landau operator. *Journal of Plasma Physics* **83** (1), 595830102.
- HUBA, J. D. 2013 *NRL Plasma Formulary, Supported by The Office of Naval Research*. Washington, DC: Naval Research Laboratory.
- JORGE, R., RICCI, P., BRUNNER, S., GAMBA, S., KONOVTETS, V., LOUREIRO, N. F., PERRONE, L. M. & TEIXEIRA, N. 2019 Linear theory of electron-plasma waves at arbitrary collisionality. *Journal of Plasma Physics* **85** (2), 905850211.
- JORGE, R., RICCI, P. & LOUREIRO, N. F. 2018 Theory of the drift-wave instability at arbitrary collisionality. *Physical Review Letters* **121**, 165001.
- JUNO, J., HAKIM, A., TENBARGE, J., SHI, E. & DORLAND, W. 2018 Discontinuous Galerkin algorithms for fully kinetic plasmas. *Journal of Computational Physics* **353**, 110–147.
- KOLESNIKOV, R.A., WANG, W.X. & HINTON, F.L. 2010 Unlike-particle collision operator for gyrokinetic particle simulations. *Journal of Computational Physics* **229** (15), 5564–5572.
- VAN LEER, B. & LO, M. 2007 A discontinuous Galerkin method for diffusion based on recovery. In *18th AIAA Computational Fluid Dynamics Conference, AIAA 2007-4083*, pp. 1–12. Miami, FL: American Institute of Aeronautics.
- VAN LEER, B. & NOMURA, S. 2005 Discontinuous Galerkin for Diffusion. In *17th AIAA Computational Fluid Dynamics Conference, AIAA 2005-5109*, pp. 1–30. Toronto, Ontario, Canada: American Institute of Aeronautics.
- LI, B. & ERNST, D. R. 2011 Gyrokinetic Fokker-Planck collision operator. *Physical Review Letters* **106** (19), 195002.
- MANDELL, N. R., HAKIM, A., HAMMETT, G. W. & FRANCISQUEZ, M. 2020 Electromagnetic full-f gyrokinetics in the tokamak edge with discontinuous Galerkin methods. *Journal of Plasma Physics* **86**, arXiv: 1908.05653.
- MORSE, T. F. 1963 Energy and momentum exchange between nonequipartition gases. *The Physics of Fluids* **6** (10), 1420–1427.
- MORSE, T. F. 1964 Kinetic model equations for a gas mixture. *The Physics of Fluids* **7** (12), 2012–2013.
- ONG, R. S. B. & YU, M. Y. 1970 The effect of velocity space diffusion on the universal instability in a plasma. *Journal of Plasma Physics* **4** (4), 729–738.
- ONG, R. S. B. & YU, M. Y. 1973 The effect of temperature perturbations on ion-acoustic and drift waves in a weakly collisional plasma. *Plasma Physics* **15** (7), 659–668.
- PAN, Q. & ERNST, D. R. 2019 Gyrokinetic Landau collision operator in conservative form. *Physical Review E* **99**, 023201.
- PAN, Q., ERNST, D. R. & CRANDALL, P. 2020 First implementation of gyrokinetic exact linearized landau collision operator and comparison with models. *Physics of Plasmas* **27**, 042307.
- PAN, Q., ERNST, D. R. & HATCH, D. 2021 Importance of gyrokinetic exact Fokker-Planck collisions in fusion plasma turbulence. *Physical Review E* **103**, L051202.
- PAN, Q., TOLD, D., SHI, E. L., HAMMETT, G. W. & JENKO, F. 2018 Full-f version of GENE for turbulence in open-field-line systems. *Physics of Plasmas* **25** (6), 062303.
- PEZZI, ORESTE, VALENTINI, F. & VELTRI, P. 2015 Collisional relaxation: Landau versus Dougherty operator. *Journal of Plasma Physics* **81** (1), 305810107.
- PUSZTAI, I., JUNO, J., BRANDENBURG, A., TENBARGE, J. M., HAKIM, A., FRANCISQUEZ, M. & SUNDSTRÖM, A. 2020 Dynamo in weakly collisional nonmagnetized plasmas impeded by landau damping of magnetic fields. *Physical Review Letters* **124**, 255102.

- ROSENBLUTH, M. N., MACDONALD, W. M. & JUDD, D. L. 1957 Fokker-Planck equation for an inverse-square force. *Physical Review* **107** (1), 1–6.
- SHI, E. L., HAMMETT, G. W., STOLTZFUS-DUECK, T. & HAKIM, A. 2019 Full-f gyrokinetic simulation of turbulence in a helical open-field-line plasma. *Physics of Plasmas* **26** (1), 012307.
- SUGAMA, H., MATSUOKA, S., SATAKE, S., NUNAMI, M. & WATANABE, T.-H. 2019 Improved linearized model collision operator for the highly collisional regime. *Physics of Plasmas* **26** (10), 102108.
- SUGAMA, H., WATANABE, T.-H. & NUNAMI, M. 2009 Linearized model collision operators for multiple ion species plasmas and gyrokinetic entropy balance equations. *Physics of Plasmas* **16** (11), 112503.
- ULBL, P., MICHELS, D. & JENKO, F. 2021 Implementation and verification of a conservative, multi-species, gyro-averaged, full-f, Lenard-Bernstein/Dougherty collision operator in the gyrokinetic code GENE-X. *Contributions to Plasma Physics* p. e202100180.